Published in final edited form as:

J Comp Neurol. 2018 October 01; 526(14): 2319–2338. doi:10.1002/cne.24501.

Neurons with diverse phenotypes project from the caudal to the rostral nucleus of the solitary tract

Susan Travers[1,4], **Joseph Breza**[1,2], **Jacob Harley**[1], **Jiulin Zhu**[1,3], and **Joseph Travers**[1]

[1]The Ohio State University College of Dentistry, Division of Biosciences

Abstract

The nucleus of the solitary tract is a potential site for taste-visceral interactions. Connections from the caudal, visceral area of the nucleus (cNST) to the rostral, gustatory zone (rNST) have been described, but the phenotype of cells giving rise to the projection(s) and their distribution among rNST subdivisions are unknown. To determine these characteristics of the intrasolitary pathway, we injected pan-neuronal and floxed AAV viruses into the cNST of mice expressing cre in glutamatergic, GABAergic or catecholaminergic neurons. Particular attention was paid to the terminal field distribution in rNST subdivisions by simultaneously visualizing P2×2 localized to gustatory afferent terminals. All three phenotypically-identified pathways terminated in rNST, with the density greatest for glutamatergic and sparsest for catecholaminergic projections, observations supported by retrograde tracing. Interestingly, cNST neurons had more prominent projections to rNST regions medial and ventral to P2×2 staining, i.e., the medial and ventral subdivisions. In addition, GABAergic neurons projected robustly to the lateral subdivision and adjacent parts of the reticular formation and spinal trigeminal nucleus. Although cNST neurons also projected to the P2×2-rich central subdivision, such projections were sparser. These findings suggest that cNST visceral signals exert stronger excitatory and inhibitory influences on local autonomic and reflex pathways associated with the medial and ventral subdivisions compared to weaker modulation of ascending pathways arising from the central subdivision and ultimately destined for the forebrain.

Graphical abstract

[4]Corresponding Author: Susan Travers, The Ohio State University, Division of Biosciences, 4151 Postle Hall, 305 West 12th Avenue, Columbus, Ohio 43210.

[2]Present address: Eastern Michigan University Department of Psychology

[3]Present Address: University of Detroit Mercy, School of Dentistry

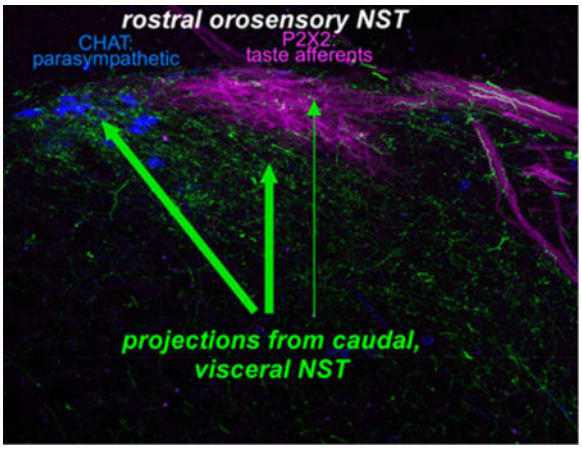

We injected AAV-GFP viruses into caudal, visceral NST and identified a topographically distinct projection to rostral, orosensory NST including glutamatergic, GABAergic, and catecholaminergic components. Terminations were notably denser in the medial and ventral than the rostral central subdivision, suggesting this pathway is more important in modulating taste-elicited autonomic and oromotor reflexes than signals in the ascending taste pathway.

Keywords

intrasolitary; rNST subdivisions; taste; visceral; RRID: AB_90738; RRID: AB_2314409; RRID: AB_390204; RRID:AB_90755; RRID: AB_221569; RRID: AB_2315161; RRID: AB_2315160; RRID: AB_2040054; RRID: AB_10013483; RRID: ISMR_JAX: 000664; RRID: ISMR_JAX 016963; RRID: ISMR_JAX: 010802; RRID MMRRC_036778-UCD; RRID: ISMR_JAX: 007908; RRID: ISMR_RBRC09645

1 INTRODUCTION

Bidirectional interactions between the sense of taste and visceral signals are well documented. Examples include the reduced consumption of preferred taste stimuli associated with visceral signals of satiety (Davis, Smith, & Singh, 2000; Sclafani, 2013) and the formation of conditioned taste aversions following gastrointestinal malaise (Garcia, Hankins, & Rusiniak, 1974), reviewed in (Reilly & Bornovalova, 2005). Similarly, gustatory stimulation can impact visceral function including the release of pancreatic insulin (Berthoud, Bereiter, Trimble, Siegel, & Jeanrenaud, 1981; Berthoud, Trimble, Siegel, Bereiter, & Jeanrenaud, 1980; Glendinning et al., 2017; Grill, Berridge, & Ganster, 1984), the acceleration of gastric emptying following oral stimulation with sweet-tasting stimuli (Inui-Yamamoto, Yuichi, & Takashi, 2009), and the suppression of gastric emptying and gastric acid production in response to bitter tastants (Inui-Yamamoto et al., 2009; Wicks, Wright, Rayment, & Spiller, 2005). The neural underpinnings of these interactions are widely distributed along the neuraxis. Although forebrain integration of taste and visceral signals is required for the expression of a conditioned taste aversion as well as the increased intake of salt following sodium depletion (Grill & Norgren, 1978; Grill, Schulkin, & Flynn, 1986), some taste-visceral interactions are mediated at the level of the brainstem. Decerebrate preparations, for example, reduce sucrose consumption in response to gastric

stretch (Grill & Norgren, 1978; Kaplan, Seeley, & Grill, 1993; Seeley, Grill, & Kaplan, 1994) and increase the intake of sweet-tasting compounds in response to insulin-induced hypoglycemia (Flynn & Grill, 1983). A role for the parabrachial nucleus (PBN) in these behaviors is suggested both by the convergence between taste and visceral signals in single neurons within the nucleus (Baird, Travers, & Travers, 2001; Hajnal, Takenouchi, & Norgren, 1999; Hermann, Kohlerman, & Rogers, 1983; Hermann & Rogers, 1985; Karimnamazi, Travers, & Travers, 2002) as well as lesion/behavioral studies, e.g. (Grigson, Reilly, Scalera, & Norgren, 1998; Reilly, Grigson, & Norgren, 1993; Scalera, Spector, & Norgren, 1995).

The rostral nucleus of the solitary tract (rNST) is another potential site for taste-visceral interactions. Although electrical stimulation of the caudal nucleus of the solitary tract (cNST) failed to modulate rNST gustatory responses (Hermann et al., 1983), a number of visceral stimuli including gastric stretch and changes in blood glucose, insulin and glucagon can all alter taste responses in rNST neurons (Bereiter, Berthoud, & Jeanrenaud, 1981; Giza, Deems, Vanderweele, & Scott, 1993; Giza, Scott, & Antonucci, 1990; Giza, Scott, & Vanderweele, 1992; Glenn & Erickson, 1976). Moreover, injections of sensitive anterograde tracers, including biotinylated dextran, Phaseolus vulgaris leucoagglutinin, or cholera toxin into the cNST at mid-postrema levels produced intrasolitary anterograde label extending to the rostral pole of the nucleus (Karimnamazi et al., 2002; Rinaman, 2010; Whitehead, Bergula, & Holliday, 2000). However, the topography of this projection was not well-described. Such details are important because the rNST is a heterogeneous structure with anatomically distinct subdivisions (Whitehead, 1990) exhibiting different patterns of inputs and outputs, neurotransmitters, and sensory characteristics, all of which suggest functional specialization. Thus, the central subdivision receives the most robust input from primary taste afferents and is the main source of ascending connections ultimately destined for the forebrain via the parabrachial nucleus. The lateral subdivision is more involved in somatosensory function, and the medial and ventral subdivisions are preferentially involved in parasympathetic and oromotor reflexes (Breza & Travers, 2016; Ganchrow et al., 2014; Halsell, Travers, & Travers, 1996; Stratford, Thompson, & Finger, 2016; Whitehead, 1993). The present study was designed to more carefully evaluate the identity of the rNST subdivisions that receive a projection from the cNST. We focused on connections originating from a level of the cNST where vagal afferents innervating the gastrointestinal tract are prominent, i.e. the medial subdivision coincident with the area postrema or just caudal to it (Hermann et al., 1983; Norgren & Smith, 1988; Shapiro & Miselis, 1985). In addition, even this restricted cNST region contains neurons with multiple phenotypes, including a vast array of peptides, as well as glutamatergic, GABAergic and catecholaminergic neurons. Previous reports have documented widespread catecholaminergic projections to the parabrachial nucleus, hypothalamus and other telencephalic structures in addition to local projections to the dorsal motor nucleus of the vagus (X) and medullary reticular formation, reviewed in (Rinaman, 2011). Local projections to X are also GABAergic and glutamatergic, reviewed in (Travagli, Hermann, Browning, & Rogers, 2006). The current paper describes similar catecholaminergic, GABAergic and glutamatergic projections to rNST and suggests that these projections differentially target the subdivisions in the NST involved in

consummatory and autonomic reflexes. A brief summary of a portion of these results appeared in a symposium report (Spector et al., 2015)

2 MATERIALS AND METHODS

2.1 Mice

For anterograde tracing from cNST, we injected cre-dependent and non-cre-dependent AAV viruses into mice expressing cre recombinase (cre) under the control of different promoters and control mice. Promoters driving cre expression included those for the 65-kd isoform of glutamic acid decarboxylase (GAD65; RRID: ISMR_JAX:010802), a synthetic enzyme for the inhibitory neurotransmitter GABA, a vesicular transporter in neurons utilizing the excitatory transmitter glutamate (VGLUT2, RRID: ISMR_JAX:016963), and dopamine beta hydroxylase (DBH, RRID: MMRRC_036778-UCD), an enzyme necessary for synthesizing norepinephrine and epinephrine. For the retrograde tracing experiments, we injected Fluorogold (FG) in "GAD67-EGFP+" mice that expressed EGFP under the control of the endogenous promoter for GAD67 (Tamamaki et al., 2003). These heterozygous mice were the positive offspring of a cross between GAD67-EGFP+ and C57BL/6J (RRID: ISMR_JAX: 000664) mice. We also utilized the negative offspring of this same cross. GAD67 is the other major synthetic enzyme for GABA. Although different isoforms of GAD were targeted for the anterograde and retrograde studies, it seems likely that these strategies identified mostly the same neurons. We base this conclusion on *in situ* hybridization reports in rats that demonstrated similar numbers and distributions of GAD65 and GAD67 neurons in NST (Stornetta & Guyenet, 1999). Moreover, we crossed mice that expressed the Venus protein under the control of the promoter for the vesicular GABA transporter (VGAT) (Y. Wang et al., 2009, RRID: ISMR_RBRC09645), found in most GABAergic neurons, with a GAD65-cre/tdTom reporter line (RRID: ISMR_JAX:007908) and observed a high degree of double labeling in NST based upon counting cells in confocal z-stacks (92.6%, 470 cells counted, one section from the mid-rNST in two mice, Fig. 1). For both the anterograde and retrograde experiments, we also used the negative offspring (GAD67-EGFP-) of crosses between GAD67-EGFP+ mice and C57BL/6J mice (RRID: ISMR_JAX:000664). ("GAD67-EGFP-"). All mice had predominantly B6 backgrounds and were adults (≥ 6 weeks). Both male and females were included in the sample. No differences were noted according to gender. Further details, including sample sizes, are included in Tables 1 and 2.

2.2 Tracer Injections

2.2.1 Anterograde Tracer Injections—Anterograde tracing from the cNST used three AAV1 viruses that drove fluorescent protein expression (Penn Vector Core). These included a neuron-specific virus driven by the synapsin promoter expressing EGFP (AAV1.hSynap.eGFP.WPRE.bGH), a floxed virus under the control of the CAG promoter (a hybrid construct consisting of the cytomegalovirus fused to the chicken-β-actin promoter) that also expressed EGFP (AAV1.CAG.Flex.eGFP.WPRE.bGH), and a second floxed virus that drove expression of both mCherry and channelrhodopsin-2 (ChR2) under the control of the chicken-β-actin (CBA) promoter. All experimental protocols were approved by the Ohio

State University Institutional Animal Care and Use Committee in accordance with guidelines established by the National Institutes of Health.

Mice were anesthetized with sodium pentobarbital (50mg/kg, i.p.) or isofluorane (1–2%), or initially with a ketamine-xylazine cocktail (100 and 10mg/kg, i.p.) with anesthesia sustained by isofluorane. Surgery was done under aseptic conditions. Following exposure of obex, a pipette (20–25μm o.d.) filled with virus was lowered into the brain, usually at ~0.2mm anterior and 0.2mm lateral to obex. We recorded neural activity through the injection pipette to determine the depth of the cNST, which was ventral to somatosensory-driven activity in the nucleus gracilis and/or dorsal to the hypoglossal nucleus, characterized by large-amplitude action potentials synchronized to respiration. In several cases, we made a second injection ~0.4mm rostral and 0.4mm lateral to obex. Except in one case where pressure was used, injections were made by iontophoresis, (5s pulses, 0.1Hz, +4–10μA for 3–12 minutes; for details see Table 1). Mice were sutured, antibiotic ointment applied to the incision, injected with a non-steroidal anti-inflammatory drug (Carprofen), and then returned to their home cage before perfusion. In the majority of cases, survival time was between 2.5–5 weeks; in a few cases, survival time was longer.

2.2.2 Retrograde Tracer Injections—Retrograde tracing from the rNST was accomplished using iontophoretic injections of 5% Fluorogold (FG: Fluorochrome, LLC, Denver, CO) dissolved in saline. Mice (7 GAD67-EGFP+ and 2 GAD67-EGFP−) were anesthetized with sodium pentobarbital (50–75mg/kg, i.p.) and the surface of the cerebellum over the rNST exposed. Gustatory responses from the anterior tongue or tactile responses from the circumvallate and foliate papillae were localized with a search electrode. Subsequently, we placed an FG-filled pipette (~20–25μm, tip diameter) at the same spot, and lowered the pipette until the dorsal border of the rNST was encountered and then the injection was typically made 50–75μm ventral to this border, in an attempt to encompass most of the dorso-ventral extent of the nucleus while limiting spread to the underlying reticular formation. In a few cases, we did not re-encounter orosensory responses but used the obvious transition from the vestibular nucleus, i.e. the cessation of large-amplitude vestibular activity as a guide for depth. Injections were made using pulsed current (5s pulses, 0.1Hz, +2–8μA, 2–15 minutes). Unlike the situation with the viral injections, where current remained stable, the current magnitude usually decreased over time when injecting FG. Mice were sutured, injected with carprofen and returned to their home cage before perfusion. Survival time ranged from 5–13 days (mean=8, s.d.= 2.4). A summary of the locations of the centers of all of the injection sites for both the retrograde tracing from the rNST and anterograde tracing from the cNST appears on a horizontal diagram (Fig. 2, adapted from Breza and Travers, 2016).

2.3 Histology

2.3.1 Perfusion and Sectioning—After deep anesthetization (ketamine/xylazine cocktail ~150 and 15mg/kg, i.p.), mice were perfused with phosphate-buffered saline (PBS),followed by a mixture of 4% paraformaldehyde, 1.4% L-lysine, and 0.2% sodium metaperiodate. Brains were extracted, post-fixed, cryoprotected overnight in a 20% sucrose-phosphate buffer (PB) solution and sectioned on a freezing microtome (30–50μm, typically

40μm) into three or four series. Sections were either immunostained and/or mounted immediately following sectioning or stored in a cryoprotectant solution at −20°C until further processing.

2.3.2 Immunohistochemistry

2.3.2.1 Anterograde tracing: For the anterograde tracing experiments, we usually analyzed native fluorescence for the EGFP-expressing viruses, but in cases with weaker labeling (DBH-cre mice and some GAD65-cre cases), we also enhanced fluorescence with immunohistochemistry for EGFP. For the mCherry-expressing viruses fluorescence was always enhanced with immunohistochemistry. In select cases, we immunostained for PHOX2b and/or P2×2 to characterize neuronal phenotype at the injection site and to specify the location of anterograde labeling from cNST relative to the primary afferent gustatory terminal field (Bartel, 2012; Breza and Travers, 2016). In a few cases, additional reactions with DAB were carried out to achieve a permanent reaction product.

2.3.2.2 Retrograde tracing: For the retrograde tracing experiments, FG was detected immunohistochemically so that retrogradely-filled cells could be viewed with a confocal microscope. Native EGFP expression in the GAD67-EGFP+ mice was sufficiently bright to identify GABAergic neurons. In most cases, tissue was also stained for PHOX2b and tyrosine hydroxylase (TH, in separate series) to further identify the phenotype of the retrogradely-labeled neurons.

2.3.1.3 General immunohistochemical procedures: The antibodies used for each case are noted in Tables 1 (anterograde tracing) and 2 (retrograde tracing), their specifications summarized in Table 3 and detailed below. The basic procedures for fluorescent immunostaining were the same for both sets of experiments and utilized free-floating sections. Briefly, we thoroughly rinsed tissue in PBS, treated it with 1% borohydride, rinsed it again, and then blocked non-specific binding sites in a mixture of 5% donkey serum and 1% bovine serum albumin in a PB/0.3% TritonX100 cocktail (blocking serum, BS). One or two primary antibodies were then added to the BS and the tissue left to incubate, either at room temperature overnight or for two-three nights at 4°C. The tissue was then thoroughly rinsed in PBS and soaked in a secondary antibody (Molecular Probes, donkey anti-rabbit or anti-sheep IgG) labeled with AF488, AF546, or AF647 at 1:500 in BS for at least three hours. We found that a prolonged incubation in the secondary antibody improved tissue penetration assessed though the confocal microscope. Sections were rinsed in PB, allowed to dry overnight, then rinsed in distilled water and coverslipped with Vectashield. Initial steps for DAB reactions were carried out in an identical manner except that a quench in H_2O_2 (0.5% in distilled H_2O, 20 min) and an additional PBS rinse was interposed before the blocking step. The secondary antibody incubation utilized a biotinylated donkey anti-rabbit IgG at a concentration of 1:500 in BS for 90 min. This was followed by a PBS rinse, incubation in the ABC compound (Vector Labs, Elite Kit, PK6100) mixed in PB and 0.01% BSA for 90 minutes, rinsed in PB, and then soaked for 15 min in 0.05% DAB with 0.02% nickel ammonium sulfate. The final reaction was initiated by adding H_2O_2 at a final concentration of 0.0015% and continued for ~1–3 minutes until optimal staining had been

achieved. The DAB cases were used to confirm what we observed with the more numerous fluorescent reactions and are not further discussed.

2.4 Antibody Characterization

2.4.1 Anti-Fluorogold: We used two antibodies against FG, one produced in guinea pig (GP, most experiments, RRID: AB_2314409) and the other in rabbit (RRID:AB_90738). According to the manufacturer, staining with the GP antibody is completely blocked by pre-incubation with FG or Fast Blue. In our lab, when we have used both antibodies in the same tissue, we have observed highly similar patterns of staining. When these antibodies were used in brains where no Fluorogold injections were made, no staining was observed.

2.4.2 Anti-tyrosine hydroxylase: Two antibodies against TH were used, both from the same manufacturer, utilizing the same antigen. Antibodies produced in either species yielded staining in the brainstem consistent with the well-known distributions of catecholaminergic neurons (Kalia, Fuxe, & Goldstein, 1985a, 1985b). The manufacturer states that Western Blot analysis indicates that both the rabbit (RRID: AB_390204) and sheep (RRID:AB_90755) antibodies react against a single band ~60–62kDa, corresponding to tyrosine hydroxylase. Our data (Fig. 3d & f) shows that this (sheep) antibody stains a subset of those cells that stain with an antibody for PHOX2b, but not with neurons that express GAD67.

2.4.3 Anti-PHOX2b: The antibody against PHOX2b was generated in the laboratory of J–F Brunet (Pattyn, Morin, Cremer, Goridis, & Brunet, 1997, RRID: AB_2315161/RRID: AB_2315160) against a sequence at the C-terminal of the molecule. This antibody stains the nuclei of a population of NST neurons which overlaps with the population of glutamatergic neurons (Kang et al., 2007), but which is mutually exclusive with cells exhibiting GABAergic markers (Fig. 3d &f). (Chen, Travers, & Travers, 2016; Kang et al., 2007).

2.4.4 Anti-EGFP: The antibody against EGFP (RRID: AB_221569) was generated against the native GFP protein. The manufacturer's data using Western blot analysis showed that the antibody was highly specific in detecting HeLa cells transfected with GFP but produced no staining in non-transfected cells. When this antibody was used with tissue in which no GFP was expressed, no staining was observed.

2.4.5 Anti-P2×2: We used an antibody to detect the P2×2 purinergic receptor (RRID: AB_2040054) which co-localizes with the distribution of primary afferent gustatory terminals in the rNST (Bartel, 2012; Ganchrow et al., 2014). The antibody was raised against the intracellular C-terminus of the receptor and data from the manufacturer show that this antibody stains a band at ~75kD, which is blocked by pre-incubation with the control peptide. Moreover, previous studies using this antibody have reported that staining is absent in mice with genetic ablation of the receptor (Finger et al., 2005).

2.5.6 Anti-mCherry: This antibody (RRID: AB10013483) was raised against DsRed-Express, a variant of Discosoma sp. red fluorescent protein; mCherry is also a variant of Discosoma sp. red fluorescent protein. The manufacturer used Western blot procedures to

test the antibody in HEK 293 cells that were transfected or not transfected with DsRed-Express, DsRed-Monomer, or AcGFP1. Staining patterns were found to be specific for the red fluorescent proteins and did not stain those cells transfected with the GFP protein or non-transfected cells. When we used this antibody with tissue in which no mCherry was expressed, no staining was observed.

2.5 Photomicroscopy and Data Analysis

2.5.1 NST divisions and subdivisions: Three major NST divisions were defined. The caudal NST (cNST) extended from the caudal border of the nucleus to the most rostral extent of the area postrema, the intermediate NST (iNST) corresponded to the nucleus that abuts the IVth ventricle and the rostral NST(rNST) began caudally when the nucleus moves lateral to the ventricle and extended to the rostral pole. Caudal and intermediate NST subdivisions were based upon the parcellation of Herbert and colleagues (Herbert, Moga, & Saper, 1990). These can be viewed in Figure 3 for a mid-postrema section, but are not typically labeled in subsequent figures so that the experimental label can be more clearly viewed. We used the nomenclature of rNST subdivisions as initially described in rats by Whitehead (Whitehead, 1990), and applied to mice by Ganchrow and colleagues (Ganchrow et al., 2014). Although these subdivisions were originally defined by cytoarchitecture and myeloarchitecture using stains for somata or myelinated fibers, our recent work suggests that immunohistochemical staining for P2×2, which identifies the terminal field of primary gustatory afferent fibers (Bartel, 2012; Breza & Travers, 2016; Ganchrow et al., 2014; Vandenbeuch et al., 2015), is an excellent marker for the (rostral) central subdivision. Thus, we delineated the central subdivision with this staining and then defined the other subdivisions in relation to it; i.e., as medial, ventral or lateral to P2×2 label. In some cases, the medial subdivision was also identified by cholinergic staining of pre-ganglionic parasympathetic neurons. It should be noted that the rostral central subdivision is distinct from the central subdivision in the intermediate/caudal NST. The intermediate/caudal central subdivision, which is prominent at the rostral pole of the area postrema, receives input from primary afferent fibers innervating the esophagus (Altschuler, Bao, Bieger, Hopkins, & Miselis, 1989) and projects strongly to the nucleus ambiguus (Herbert et al., 1990; Ross, Ruggiero, & Reis, 1985), but in marked contrast to the rostral central NST (Halsell et al., 1996; Whitehead, 1990), does not project to the parabrachial nucleus (Herbert et al., 1990).

2.5.2 Anterograde experiments: Photomicrographs were taken using a Nikon E600 Ellipse light fluorescent microscope (4–10× lenses; fluorescent filters: 450–490nm ex, 500–560nm ba to view EGFP or AF488; 520–560nm ex, 590–650nm ba to view mCherry or AF546) or with an Olympus confocal microscope (FV1000 or FV3000). Confocal photomicrographs (z=2μm) were taken with a 20× lens at a resolution of 0.621 μm/pixel using an argon laser exciting at 488 nm for GFP and AF488, a HeNe laser exciting at 543 for AF546 and a 635nm diode to detect far-red AF647 fluorescence. Additional confocal micrographs (z=1μm) were taken using 20×, 40× or 60× lenses with a digital zooms ranging from 1–3× (0.069–.310 μm/pixel resolution). We focused on the center of the injection site in cNST and on a level of the rNST midway between where the NST moves away from the IVth ventricle and the rostral pole. In select cases, additional photomicrographs were taken to further assess the extent of the injection or projection regions. We took darkfield or differential

interference contrast (DIC) photomicrographs along with the fluorescent images to aid in delineating NST borders, based mainly upon the contrast between the poorly myelinated NST and surrounding regions. Maximum-intensity projections were created using Olympus Fluoview (Version 4.2a or 31S) software or in Image J and contrast and brightness were adjusted. For the 20× confocal images of the injection site and rostral NST, it was usually necessary to make a composite of two overlapping z-stacks, using the 3-D stitching module in Image J. Unless otherwise specified in the figure captions, maximum intensity projections included sections from the entire confocal stack. In a few cases, obvious particulate artifact arising from the secondary antibody was removed with the "remove noise" filter in Image J. Images were brought into Canvas (ACD Systems, v10) for final assembly of panels.

2.5.3 Retrograde Experiments: Photomicrographs of FG at the injection site center, along with a darkfield image were taken using the Nikon fluorescent microscope described above at magnifications of 4× and 10×. We photographed native FG at the injection site (325–375ex, LP400ba) because the native tracer appeared just as bright (if not brighter) than the immunohistochemically detected product at this magnification. The approximate extents of the injection site "cores", characterized by densely-distributed labeled neurons, neuropil, and between-cell fluorescence, and "shells", with more scattered labeled cells and neuropil were manually outlined from the photomicrographs and the outlines of the NST were drawn based upon the darkfield images which highlight myeloarchitecture. Summaries of injection site centers were plotted on both the horizontal diagram in Figure 2 and on a standard set of coronal sections prepared in our lab with black-gold staining, a procedure that highlights myelin and thus the NST borders (Corson et al., 2012; Schmued and Slikker, 1999). Confocal photomicrographs of retrogradely-labeled cells were taken at 20×, z=2μm, using appropriate filters (described above) to detect immunohistochemically detected FG, PHOX2b, TH, and native EGFP in GAD67 neurons. We counted retrograde labeling at two levels of cNST: obex and at the mid-point of area postrema ("mid-AP"). To capture the entire NST at this magnification, it was usually necessary to make a composite of two overlapping z-stacks. Z-stacks were brought into Image J, converted into 8-bit images and then stitched into a composite z-stack using the 3-D stitching module. DIC photomicrographs were taken along with the confocal fluorescent images to aid in delineating anatomical borders. Retrogradely labeled cells were first plotted by consulting only the FG channel of the composite z-stacks and then cells were classified as single- or double-labeled for the other markers.

3 RESULTS

3.1 Anterograde tracing with AAV viruses

3.1.1 Pan-neuronal promoter—Initial tracing studies used an AAV1 virus driving EGFP expression under the control of the synapsin promoter in order to estimate the full extent of a projection from cNST to rNST (n=2). Labeled somata at the injection sites were centered medial to the solitary tract at the level of obex or caudal area postrema (AP, Fig. 2). Figure 4 shows an injection centered in the medial subnucleus that also encompassed the dorsomedial and commissural subnuclei and extended lateral to the solitary tract into the ventrolateral subnucleus. A few EGFP positive cells were also observed in the AP. Although some labeled

somata were also apparent in the dorsal motor nucleus of the vagus (X) and hypoglossal nucleus (XII), neither of these populations are likely to give rise to central projections because they are preganglionic parasympathetic and motor neurons that send projections to peripheral targets. In the horizontal plane, somal labeling extended for approximately 500μm but was most dense at caudal levels of the area postrema and obex and virtually absent in the NST rostral to the area postrema. Therefore, the NST injection site was confined to the caudal division. At the most rostral level shown, near the rostral pole of the area postrema, there were just a few scattered somata. Interestingly, at this level, anterograde label fills most of the nucleus but was virtually absent in the central subnucleus (Fig. 4b, arrowheads). Thus, even this close to the injection site, specific patterns of intranuclear connectivity were revealed. Anterograde labeling was also present throughout the intermediate division of the nucleus (not shown) and extended into the rNST.

Figure 5a shows confocal photomicrographs of anterograde viral label at three levels of rNST, one just rostral to where the NST abuts the IVth ventricle (Fig. $5a_1$), a second at a mid-level of rNST (Fig. $5a_2$) and a third close to the rostral pole of the nucleus (Fig $5a_3$). Afferent fibers and varicosities were present throughout the rNST in a caudal (most dense) to rostral (least dense) gradient. In addition, fibers and varicosities extended into the underlying reticular formation. Figure 5b shows the same sections immunostained for P2×2, and for CHAT. Projections from the cNST were notably denser ventral and medial to the strongest P2×2 staining; i.e., projections were stronger to the medial and ventral than to the central subdivision. Moreover, the medial terminal field overlapped extensively with CHAT-stained neurons. Figure 5c shows higher power-confocal images of a different (adjacent) section from the mid-rNST. Panel $5c_1$ is centered at the ventral edge of the P2×2 and shows that varicosities were evident in the P2×2 field though were much heavier ventrally. Panel $5c_2$ is centered on the medial subdivision of this same section and illustrates the extensive intermingling of afferent labeling from the cNST with preganglionic parasympathetic neurons, including a few appositions of varicosities with soma or presumed dendrites (see magnified inset in panel c_3).

3.1.2 Cre-dependent virus tracing in VGLUT2-cre, GAD65-cre, and DBH-cre mice—

To determine some of the phenotypes of cNST neurons that project to rNST, we made injections of cre-dependent viruses in mice that expressed cre in different cell types: excitatory glutamatergic neurons, inhibitory GABAergic neurons, and catecholaminergic A2 neurons. Projections from cNST to rNST were evident for each phenotype, but varied in terms of magnitude and pattern.

3.1.2.1 Glutamatergic projections: To identify glutamatergic projections, injections were made in three VGLUT2-cre mice, two with a virus expressing EGFP under the control of the CAG promoter and one that expressed mCherry (as well as ChR2) under the control of the CBA promoter. Although the overall patterns were similar for both viruses, label was stronger for the CAG-EGFP virus and low magnification images giving an overview of the injection site and resulting anterograde label for one of those cases is illustrated in Figure 6a and c. Corresponding high magnification images appear in Figures $6a_1$, $6a_2$, and $6c_1$. Control injections of the CAG virus into mice that did not express the cre protein (n=2) led

to negligible somal labeling at the injection site and no anterograde label. Figure 6a and 6a$_1$ shows the center of an injection site in a VGLUT2-cre mouse centered medial to the solitary tract at a level just caudal to the AP. Labeled cells extended lateral to the tract as well as into the AP and contralateral NST, and some somal labeling was evident in the overlying nucleus gracilis and underlying reticular formation. Label in the overlying gracilis likely represents diffusion of the virus along the pipette. The source of labeled cells in the subjacent reticular formation, however, is more likely a consequence of transport by dendrites that extend into the overlying nucleus since a number of RF dendrites can be seen extending in the dorsal direction (Fig. 6a$_2$, arrowheads). Moreover, the rotundus component of the cuneate nucleus, which is also adjacent to the cNST and which contains plentiful VGLUT2-expressing neurons (Allen Mouse Brain Atlas ISH Data) is devoid of EGFP-expressing cells (Fig. 6a). In contrast to the injection sites for non-specific viral injections (Fig. 4), there was a notable paucity of labeled somata in (cholinergic) X and XII, attesting to the specificity of viral transduction (Fig. 6a and 6a$_1$). The topography of the terminal field following injections in VGLUT2 mice appeared very similar to those following non-specific AAV viral injections. Terminals were evident throughout the nucleus with the most robust projections in the medial and ventral subdivisions (Fig. 6c, 6c$_1$), a conclusion substantiated in a second case (SL15–57, not shown) with P2×2 immunostaining. There was also intense labeling in incoming primary afferent fiber fascicles, presumably in the Xth nerve (Fig. 4c, arrowhead). In the underlying reticular formation, there was strong fluorescence in fibers of passage as well as many varicosities, suggestive of terminations.

3.1.2.2 GABAergic projections: Injections in the cNST of GAD65-cre mice (N = 9) were made with the same two viruses used in the VGLUT2 studies with comparable anatomical coordinates and injection parameters. Despite these similarities, injection sites were smaller in the GAD65 cre line, and the virus tended to be expressed by cells located more laterally and ventrally in the nucleus (Fig. 6b, 6b$_1$). Moreover, although reticular neurons just lateral to NST were usually included in the injection site, labeled cell bodies in the intermediate and dorsal reticular formation that were so prominent in the VGLUT2-cre mice were not evident in the GAD65-cre cases. To verify phenotype specificity, sections from five GAD65-cre cases were also immunostained for PHOX2b, a putative marker for excitatory neurons in NST (Kang et al., 2007). Counts of labeled neurons from the center of these injection sites showed that, across all cases, only 4.6% of 928 NST virally-labeled cells were double-labeled with PHOX2b, indicating a high degree of specificity (Fig. 7b$_1$ – b$_3$). In contrast, 67.1% of neurons were double-labeled for PHOX2b in one of the VLGLUT2 cases (Fig. 7a$_1$ – a$_3$).

Although injection site sizes and the magnitude of anterograde labeling varied across the seven GAD65-cre cases, the patterns of anterograde labeling were consistent. Similar to projections from VGLUT2 neurons, anterograde projections from GAD65 neurons were denser in the medial and ventral subdivisions compared to the central subdivision, although labeling in all these subdivisions was usually lighter than in the VGLUT2 or non-specific viral cases (Fig. 6d, 6d$_1$). In addition, in contrast to the glutamatergic projections, GABAergic projections were markedly more robust in the lateral subdivision of rNST as well as lateral to the rNST itself in the parvicellular reticular formation. This subnuclear

pattern of labeling was verified in a second case with P2×2 immunostaining (not shown). In the cases with the largest injections, projections extended to the spinal trigeminal nucleus (Fig. 6d, 6d1). Overall, labeled fibers in the solitary tract and those traveling though the reticular formation ventral to the NST were much less striking compared to injections in VGLUT2-cre mice. One injection (not shown) labeled just a handful of somata restricted to the ventral and lateral regions of cNST and extended into the adjacent reticular formation, a region corresponding to nucleus intermedius (Edwards, Deuchars, & Deuchars, 2009). In this case, anterograde labeling was apparent in the lateral and ventral rNST, as well as in the reticular formation and trigeminal nucleus. Projections to the medial rNST, however were not observed, further suggesting a specific topography of intranuclear connectivity.

3.1.2.3 Catecholaminergic Projections: To identify catecholamineric projections, we injected the same two viruses into 3 mice expressing cre under the control of the DBH promoter (AAV-CAG-EGFP, n=2; AAV1-CBA-ChR2-mCherry, n=1). Injection sites were robust and located in a similar region of cNST as the injections described above; i.e. centered at the level of obex or area postrema (Fig. $6a_1 – a_3$). In contrast to injections made in the VGLUT2-cre and GAD65-cre mice, however, there were relatively few labeled neurons in the reticular formation ventral or lateral to the nucleus or in the overlying dorsal column nuclei. Nevertheless, a small number of more faintly labeled cells could be distinguished in the hypoglossal nucleus. In two cases, sections were immunostained with an antibody against TH. Counts of virally-labeled neurons in NST suggested that the specificity of viral expression was a function of the intensity of viral expression. Intensity was approximated using a built-in feature of the cell counter plug-in in Image J that reports intensity associated with the location of a given plotted cell. The mean intensity of viral labeling for double-labeled cells was over 3× as great as that exhibited by single-labeled cells ($\bar{X}$ = 163.9 ± 92.8 s.d. vs 50.3 ± 66.4, T test, P<.00001). Moreover, the intensity of viral expression showed a clear bimodal distribution. Across the two cases, only a minority of the neurons that were weakly labeled for the virus co-expressed TH (26/136, 19%), whereas the majority of strongly labeled neurons immunostained with the TH antibody (44/60, 73%, X^2=53.3, P<.0005). Figure 8 ($a_1 – a_3$) shows photomicrographs taken near the center of the injection site for one case immunostained for TH, demonstrating that most neurons that strongly expressed the virus were double-labeled for TH. Panels $8b_1 – b_3$ show photomicrographs of anterograde labeling resulting from this injection. Although catecholaminergic projections to rNST had similar patterns as glutamatergic and GABAergic projections, they were markedly sparser. Nevertheless, varicosities that were double-labeled for EGFP and TH could be detected in rNST. Consistent with the observation that the injection site containned some neurons singly-labeled for the virus, however, singly-labeled viral fibers and varicosities were also observed. Moreover, many rNST fibers and varicosities were singly labeled for TH, suggesting a source of catecholaminergic innervation from sources other than cNST.

3.1.3 Retrograde Tracing with Fluorogold—The neurotransmitter phenotypes of projections from the caudal to the rostral NST were also assessed used the retrograde marker FG. These injections were made under electrophysiological guidance in either mice expressing EGFP under the control of the endogenous promoter for GAD67 (GAD67-EGFP

+, n=7), or the negative offspring of this same cross (n=2). The phenotype of retrogradely labeled neurons was then assessed by identifying FG labeled neurons in EGFP-expressing neurons in the GAD67-EGFP+ mice, and/or following immunostaining for tyrosine hydroxylase (n=8), and PHOX2b (n=4), (See Table 2).

Figure 9 illustrates a case where an injection was made at an rNST site that responded to gustatory stimulation of the anterior tongue (Fig. 9a). The injection appeared centered in the central subdivision but spread to the other subdivisions as well, and more weakly to the surrounding vestibular nucleus and reticular formation. Similar spread across subdivisions was observed in the other cases; no injections were confined to a single subdivision. Caudal to the injection site, retrogradely labeled neurons in the NST were evident in a continuous distribution that diminished systematically at more caudal locations, but which typically extended to the level of obex (Fig. 9b). Across all cases, counts of retrogradely-labeled neurons at obex and mid-postremal levels (levels coincident with our anterograde injection sites), revealed an average of 133 ± 36.2 (s.e.) neurons, summed across the two levels. As evident in Figure 10, however, the number of retrogradely-labeled neurons varied markedly. The oral responsiveness of each of the injection sites and the locations of the injection site centers in the horizontal and coronal planes are presented in Figures 2 and 10; Figure 10 also summarizes the relative sizes of these injections. Two injections were centered at the rostral pole of the nucleus in locations responsive to anterior tongue taste stimulation, five at sites further caudal and medial that responded to mechanical stimulation of the circumvallate and/or foliate papillae, and two at unresponsive sites located at the medial pole of the nucleus. Although the possibility of fluid aspiration precluded gustatory stimulation of the posterior tongue, the two posterior-responsive sites may also have been gustatory responsive (Breza & Travers, 2016; Travers & Norgren, 1995). Not surprisingly, there was a significant positive correlation (+0.79, P=.01, Pearson's r) between the sizes of the injection sites and the numbers of labeled neurons. If the case with the largest injection is not included, this correlation remained positive, but became non-significant (+0.55, P>.1), suggesting that other factors contributed, e.g. injection site location within the nucleus.

Retrogradely-labeled neurons of each of the three phenotypes examined were observed. Across all cases, the proportions of double-labeled neurons were consistent with the anterograde observations: PHOX2b neurons were most prominent ($\bar{X}$ = 56 ± 2.3 [s.e.]%), GAD67 neurons made a substantial contribution ($\bar{X}$ = 26 ± 3.1 [s.e.]%) and TH-positive neurons had a modest representation ($\bar{X}$ = 10 ± 1.7 [s.e.]%). Figure 9c and d shows examples of retrogradely-labeled neurons that were double-labeled for GAD67 or PHOX2b (this case was not immunostained for TH).

4 DISCUSSION

The present study details a projection from the caudal, visceral NST to the rostral, orosensory region of the nucleus. Extending earlier observations (Karimnamazi et al., 2002; Rinaman, 2010, Whitehead et al., 2000), we show a differential pattern of projections originating from three neurotransmitter defined phenotypes, presumed excitatory cells expressing the glutamate transporter VGLUT2, inhibitory cells expressing synthetic enzymes for GABA, and a small population of catecholaminergic neurons. In general,

projections were considerably denser to the medial and ventral subdivisions in rNST, and notably sparser, though present in the central subdivision. Unlike either the glutamatergic or catecholaminergic projections, cNST GABAergic neurons had a pronounced projection to the lateral subdivision. The prominent projections to the medial and ventral subdivisions suggest that the cNST differentially influences rNST neurons involved with visceral and reflex functions.

4.1 Technical Issues

4.1.1 Viral Transport to Primary Afferents—We noted that some injections of AAV viruses in the cNST appeared to label incoming afferent axons at the same levels of the rNST where anterograde label was present. This was particularly true with the use of either promiscuous or VGLUT2-driven viruses (Fig. 6c), and likely resulted from viral uptake by afferent nerve terminals at the level of the (caudal) injection site. This raises the possibility that a significant proportion of the rNST terminal label that we observed was derived from collateral projections of vagal afferent fibers which terminated at rostral levels. This interpretation, however, seems unlikely based on previous tracing studies of the vagus nerve or visceral end organs which have consistently demonstrated that vagal terminations are restricted to cNST, e.g. (Gwyn, Leslie, & Hopkins, 1985; Hamilton & Norgren, 1984; Shapiro & Miselis, 1985). Although tracers injected directly into the vagal (nodose) ganglion have been observed to produce terminal fields which sometimes extended to rostral levels of the nucleus, (Chang, Strochlic, Williams, Umans, & Liberles, 2015; Contreras, Beckstead, & Norgren, 1982; Williams et al., 2016), these more rostral terminal fields were likely due to tracer spread to the petrosal ganglion which contains somata of glossopharyngeal afferents and which is contiguous to the nodose ganglion (see e.g., Fig. 6 in (Altschuler et al., 1989)). Thus, although it is likely that the viral labeling in incoming afferents that we observed includes vagal fibers, it seems most parsimonious to conclude that these largely terminate in cNST and that the majority of rNST anterograde label arose from cNST neurons. This conclusion is supported by our retrograde tracing experiments.

4.1.2 Specificity of Cre-Dependent Viral Expression—The expression of the cre-dependent AAV viruses employed in the present study relied on cre expression and, for the most part, faithfully corresponded to the intended phenotypes. Control injections of a cre-dependent virus into mice that did not express cre produced only a few very faintly labeled neurons and no anterograde label. Further, cre-dependent cNST viral injections in GAD65-cre mice labeled cells that rarely immunostained for PHOX2b, a transcription factor absent in inhibitory NST neurons, but present in many (though not all) neurons expressing VGLUT2 (Stornetta, Sevigny, & Guyenet, 2002). Indeed, in the present study, a majority of virally-labeled somata following a cNST injection into VGLUT2-cre mouse were positive for PHOX2b. The specificity of similar injections into a DBH-cre line was more complex and related to the intensity of viral expression, which was bimodally distributed. Only a minority of weakly-labeled neurons immunostained for TH. In contrast, a majority with robust viral labeling were double-labeled for this catecholamine. Nevertheless, the proportion of double-labeled cells (73%) was lower than reported in a previous study in the rostral ventrolateral medulla (>90%) that also used a cre-dependent AAV virus, a mouse with the same transgene, and the same antibody (Abbott et al., 2013). Differences in the

viral serotype (I vs II), promoter (CAG versus EF1), background strain of mouse, or brainstem location could have contributed to the lower proportion of our neurons that co-labeled for TH. Although the lack of complete co-expression could imply less specific viral induction, it is also possible that the antibody did not detect all cells expressing DBH. We used a TH rather than a DBH antibody because we were unable to locate an effective DBH antibody for mouse. However, in other experiments performed in our lab in rat (unpublished observations), we noted that despite robust staining, this TH antibody only labeled about 65% of the neurons that immunostained for DBH using a very well characterized DBH antibody (e.g., (Kreisler, Davis, & Rinaman, 2014; Rinaman, 2003)). Thus, our estimate of double-labeled neurons with the TH antibody is probably somewhat low. In any case, because we observed varicosities double-stained for both TH and the virus in the rNST following cNST injections into DBH-cre mice (Fig. 8), and because TH neurons were retrogradely labeled after rNST FG injections, our conclusion that there is a sparse catecholaminergic caudal to rostral NST projection is unaltered.

4.2 Phenotypes of cNST-rNST projections

Our data indicate that the caudal to rostral intrasolitary projection is phenotypically heterogeneous, comprised of neurons expressing VGLUT2, GAD65/67, and the catecholamines. The A2 catecholaminergic neurons include a subset of the glutamatergic population in the cNST (Stornetta et al., 2002), and are well-known to respond to a variety of gut-related, interoceptive and behavioral stimuli that inhibit feeding behavior, as well as respiratory and cardiovascular signals (reviewed in (Rinaman, 2011)). Although our data suggest that there is an A2 projection to rNST, implying that such visceral signals could affect the rNST orosensory and autonomic circuitry, this projection was sparse, indicating only a modest influence from this particular population of cells. Projections from GABAergic and especially glutamatergic cNST neurons were more robust. For these two phenotypes, there were notable differences in the pattern of terminal field projections and the location of cNST neurons from which the projections originated. Although we used very similar stereotaxic coordinates, viruses, and injection parameters in the GAD65- and VGLUT2-cre mice, injection sites in the GAD65 mice were typically smaller and more ventrolaterally restricted (Fig. 6). These differences are consistent with previous reports of the relative densities of GAD- and VGLUT2-expressing neurons in cNST (Okada et al., 2008), as well as our observations in the cNST of GAD67-EGFP+ mice with immunostaining for the excitatory marker, PHOX2b (Fig. 3). Nevertheless, although both excitatory and inhibitory projections originate from somewhat spatially distinct populations in cNST, they both targeted the medial pole of rNST and the ventral subdivision. In addition, GAD65 neurons targeted the lateral subdivision of rNST and the ventrolaterally adjacent reticular formation, a distribution that extended into the subnucleus oralis of the trigeminal complex. A previous study in rat using classic anterograde and retrograde techniques also described cNST projections from all NST levels to the sensory trigeminal complex, although projections arising from cNST at the level of the area postrema were sparser and more confined to the caudal part of the complex than what we observed (Zerari-Mailly, Buisseret, Buisseret- Delmas, & Nosjean, 2005). Thus, our results suggest that projections to the lateral NST and adjacent areas arise preferentially from GABAergic neurons. Because oral tactile responses predominate in the most lateral rNST and extend into the adjacent regions (Breza

& Travers, 2016), there is the potential for inhibitory modulation of oral somatosensory responses by visceral signals arising from cNST.

4.3 Functional Significance of the Anatomical Pattern

The medial subdivision of rNST was a prominent target for all of the phenotypically defined intrasolitary projection neurons we identified in cNST. This result is consistent with what can be gleaned from photomicrographs and brief descriptions in previous reports (Karimnamazi et al., 2002; Rinaman, 2010; Whitehead et al., 2000). Neurons within the medial subdivision include cholinergic pre-ganglionic parasympathetic neurons (PGPs), which have axons that travel in the IXth and Xth cranial nerves to innervate salivary glands (Contreras, Gomez, & Norgren, 1980; Stratford et al., 2016). The most anterior PGPs have axons in the IXth nerve that innervate Von Ebner's salivary glands in the posterior tongue (Bradley, Mistretta, Bates, & Killackey, 1985), and are continuous caudally with PGPs projecting axons in the superior laryngeal and cervical branches of the vagus, including those that supply minor salivary glands extending from the pharynx to the esophagus (Contreras et al., 1980; Hamilton & Norgren, 1984). Indeed, although most PGPs that travel in the subdiaphragmatic vagus are confined to the dorsal motor nucleus of the vagus abutting the caudal NST, some of these too extend to the rostral zone of the nucleus (Norgren & Smith, 1988). Results from double-labeling with a CHAT antibody revealed that rostral medial cholinergic cells intermingle with profuse varicosities arising from the cNST that and that some appear to contact the somata and dendrites (Fig. $5c_2$ and $5c_3$), suggesting a robust influence of visceral signals on these parasympathetic neurons. Although frank gustatory responses are sparse in the medial subdivision, consistent with evidence for weak primary afferent input (Breza & Travers, 2016; Ganchrow et al., 2014; Whitehead, 1988), dendrites from PGPs at the rostral pole of NST extend laterally into the zone of primary afferent terminations (Kim, Chiego, & Bradley, 2004). Thus, these rostral PGPs are in a position to be modulated by both taste and visceral signals, consistent with observations that both types of signals can modulate salivation (Gjorstrup, 1980; Hockman, Hagstrom, & Hoff, 1965; Kawamura & Yamamoto, 1978; Matsuo et al., 2001; Ueda et al., 2016) and other functions, including gastric motility (Inui-Yamamoto et al., 2009; Wicks et al., 2005).

The ventral subdivision of rNST also receives a robust cNST projection. This region is subjacent to the dense primary afferent input located in the central subdivision but some taste responses have been noted there (Geran & Travers, 2006; Hu, Travers, & Travers, 1997; McPheeters et al., 1990), perhaps due to monosynaptic input onto dorsally-extending dendrites (Corson & Bradley, 2013; M. Wang & Bradley, 2010). The ventral subdivision projects preferentially to the underlying reticular formation (Halsell et al., 1996), which houses circuitry implicated in the consummatory phase of feeding, including stereotyped taste-modulated acceptance and rejection behaviors; i.e. licking, swallowing and oral rejection ("gaping") (Chen, Travers, & Travers, 2001). Abundant data demonstrate that visceral signals can both inhibit and potentiate taste-modulated consummatory behaviors, consistent with the presence of both glutamatergic and GABAergic cNST projections to rNST. For example, caloric substances such as sugars and lipids can act on receptors in the intestine to suppress (satiety), e.g., (Davis & Perez, 1993; Spector, Klumpp, & Kaplan, 1998) or potentiate (appetition) intake (Schier & Spector, 2016; Sclafani, 2013). Similarly,

infusing nausea-inducing ligands into the gut, including LiCl or bitter stimuli, had similar rapid inhibitory effects on consummatory behavior (Schier, Davidson, & Powley, 2011), but potentiated gaping (Schier & Spector, 2016).

Although projections from the cNST to the rNST favored the medial and ventral subdivisions, the central subdivision where P2×2 staining was prominent also received projections, including anterogradely-labeled fibers with varicosities, consistent with a functional connection (Fig. $5c_1$). The central subdivision is the main target of primary afferent gustatory fibers in the VIIth and IXth cranial nerves (Whitehead, 1986) and appears to be the dominant location where taste responses are recorded, at least in acute neurophysiological preparations (Breza & Travers, 2016; Geran & Travers, 2006; Yokota, Eguchi, & Hiraba, 2014). Neurons in this region are the major source of the ascending pathway to the parabrachial nucleus (Halsell et al., 1996; Whitehead, 1990), which in turn gives rise to thalamocortical and subcortical forebrain projections (Norgren, 1976). Thus, the current data indicate that at least to a modest extent, visceral signals from cNST could modulate ascending taste information ultimately used in more complex functions like perception, motivation, and learning.

Indeed, previous studies have reported that rNST taste responses (likely recorded in the central subdivision) can be inhibited by gastric stretch (Glenn & Erickson, 1976), as well as increases in blood glucose, insulin and glucagon (Giza et al., 1993; Giza & Scott, 1983, 1987; Giza et al., 1992). Although the caudal to rostral intrasolitary pathway is a potential candidate substrate at least partially underlying such effects, other studies have failed to find an influence of electrical stimulation of either the vagus nerve or caudal NST on rNST taste activity (Hermann et al., 1983). This is consistent with our observations that cNST projections to the central subdivision are considerably weaker than projections to more medial and ventral subdivisions. Overall then, our results suggest that rather than primarily modulating taste signals destined for the forebrain, cNST projections to rNST preferentially target neurons involved in local reflex function, i.e. reflexive parasympathetic activity via the medial subdivision (salivary secretions along the upper GI tract, gastric motility, gastric acid and insulin release) and oromotor acceptance and rejection responses via the ventral subdivision. Stronger modulation of signals destined for the forebrain seems more likely to occur at the next level of the neuraxis, the parabrachial nucleus. Indeed, unlike the NST, a previous study demonstrated that single parabrachial neurons can be co-activated by taste stimulation and electrical stimulation of the cNST (Hermann et al., 1983). Moreover, pontine taste responses are modulated by gastric inflation (Baird et al., 2001) and sucrose-selective neurons in the PBN are profoundly depressed by intraduodenal lipid (Hajnal et al., 1999). In line with these physiological observations, anatomical data suggests convergence of projections from the cNST and rNST in the “waist area” of the parabrachial nucleus (Hermann et al., 1983; Karimnamazi et al., 2002); i.e., the classic “pontine taste area” (Norgren & Pfaffmann, 1975).

4.3 Multiple Functions of the Taste System

Besides providing evidence for intrasolitary connections, the present study reinforces the notion that the taste system serves multiple functions (e.g., (Spector & Travers, 2005)), and

that parallel processing is initiated at the first central relay (Zaidi, Todd, Enquist, & Whitehead, 2008). Interestingly, evidence for an analogous division in other types of modulatory function is provided by data on neuropeptides and anatomical studies of descending projections to rNST. Immunohistochemical data suggest that several peptidergic systems, including a number that impact feeding and digestion, such as neuropeptide Y and the endogenous opiates (N. R. Kinzeler & Travers, 2008; Kotz, Billington, & Levine, 1997; Stanley, Kyrkouli, Lampert, & Leibowitz, 1986; Taylor, Lester, Hudson, & Ritter, 2007) preferentially target subdivisions other than the central. Thus, fibers expressing neuropeptide Y and galanin were prominent medial to P2×2 staining, while calcitonin gene-related peptide flanked the primary afferent terminal field laterally (Stratford et al., 2016). Likewise, fibers immunopositive for enkephalin were prominent in the medial NST and ventral NST (Fallon & Leslie, 1986), compared to the more dorsolateral portions of the nucleus, with both enkephalin and endomorphin fibers much sparser in the P2×2 field (N.R. Kinzeler, 2011). A similar medial/ventral bias was described for the distribution of substance P fibers in the gustatory zone of NST (Harrison, Hoover, & King, 2004).

Anterograde tracing from the forebrain similarly reveals that the medial and ventral subdivisions are preferentially innervated by descending inputs from subcortical forebrain regions. This is particularly clear in the case of the bed nucleus of the stria terminalis and central nucleus of the amygdala (Danielsen, Magnuson, & Gray, 1989; Halsell, 1998; van der Kooy, Koda, McGinty, Gerfen, & Bloom, 1984), an amygdalar region reported to modulate taste reactivity (Riley & King, 2013) and motivational aspects of feeding (e.g., (Warlow, Robinson, & Berridge, 2017)). On the other hand, while the central subdivision is relatively spared from several modulatory influences, descending projections from the primary gustatory cortex in the insula prominently target this subdivision, which houses the neurons whose signals ultimately reach this same region of cortex (Hayama & Ogawa, 2001; Whitehead et al., 2000). Thus, despite being relatively isolated from direct cNST, peptidergic and subcortical influences, the central subdivision appears intimately involved in a reciprocal processing loop with the primary gustatory cortex, a region hypothesized to underlie complex perceptual functions such as discrimination, learning, and the multisensory integration that underlies flavor (e.g., (de Araujo, Geha, & Small, 2012; Maier, 2017; Samuelsen & Fontanini, 2017)).

Acknowledgments

This work was supported by NIH RO1 DC00614 and RO1 DC016112 to ST and R21 013676 to JT and a seed grant from the Ohio State University College of Dentistry. We thank Dr. Francois Brunet for the gift of the primary antibody against PHOX2b and Dr. Yuchio Yanagawa for the gift of the breeding stock for the GAD67-EGFP mice. The Venus fluorescent protein was developed by Dr. Atsushi Miyawaki at the RIKEN Brain Science Institute in Wako Japan; the VGAT-VENUS transgenic mouse developed by Dr. Yuchio Yanagawa was made available to us from Dr. Hisashi Umemori at the University of Michigan Medical School, Ann Arbor Michigan. The confocal images presented in this report were generated using the instruments and services at the Campus Microscopy and Imaging Facility, The Ohio State University, particular thanks go to Mr. Brian Kennemoe and Dr. Sara Cole for training and advice. The CMIF facility is supported in part by grant P30 CA016058, National Cancer Institute, Bethesda. The excellent technical assistance of Grace Houser and Cemaliye Semmedi is greatly appreciated.

References

Abbott SB, DePuy SD, Nguyen T, Coates MB, Stornetta RL, Guyenet PG. Selective optogenetic activation of rostral ventrolateral medullary catecholaminergic neurons produces cardiorespiratory stimulation in conscious mice. J Neurosci. 2013; 33(7):3164–3177. [PubMed: 23407970]

Allen Brain Atlas ISH Data. from http://mouse.brain-map.org/search/index

Altschuler SM, Bao XM, Bieger D, Hopkins DA, Miselis RR. Viscerotopic representation of the upper alimentary tract in the rat: sensory ganglia and nuclei of the solitary and spinal trigeminal tracts. J Comp Neurol. 1989; 283(2):248–268. [PubMed: 2738198]

Baird JP, Travers SP, Travers JB. Integration of gastric distension and gustatory responses in the parabrachial nucleus. Am J Physiol Regul Integr Comp Physiol. 2001; 281(5):R1581–1593. [PubMed: 11641131]

Bartel DL. Glial responses after chorda tympani nerve injury. J Comp Neurol. 2012; 520(12):2712–2729. [PubMed: 22315167]

Bereiter DA, Berthoud HR, Jeanrenaud B. Chorda tympani and vagus nerve convergence onto caudal brain stem neurons in the rat. Brain Res Bull. 1981; 7(3):261–266. [PubMed: 7272802]

Berthoud HR, Bereiter DA, Trimble ER, Siegel EG, Jeanrenaud B. Cephalic phase, reflex insulin secretion. Neuroanatomical and physiological characterization. Diabetologia. 1981; 20(Suppl):393–401.

Berthoud HR, Trimble ER, Siegel EG, Bereiter DA, Jeanrenaud B. Cephalic-phase insulin secretion in normal and pancreatic islet-transplanted rats. Am J Physiol. 1980; 238(4):E336–340. [PubMed: 6769337]

Bradley RM, Mistretta CM, Bates CA, Killackey HP. Transganglionic transport of HRP from the circumvallate papilla of the rat. Brain Res. 1985; 361(1–2):154–161. [PubMed: 2417659]

Breza JM, Travers SP. P2×2 Receptor Terminal Field Demarcates a "Transition Zone" for Gustatory and Mechanosensory Processing in the Mouse Nucleus Tractus Solitarius. Chem Senses. 2016; 41(6):515–524. DOI: 10.1093/chemse/bjw055 [PubMed: 27131102]

Chang RB, Strochlic DE, Williams EK, Umans BD, Liberles SD. Vagal Sensory Neuron Subtypes that Differentially Control Breathing. Cell. 2015; 161(3):622–633. DOI: 10.1016/j.cell.2015.03.022 [PubMed: 25892222]

Chen Z, Travers SP, Travers JB. Muscimol infusions in the brain stem reticular formation reversibly block ingestion in the awake rat. Am J Physiol Regul Integr Comp Physiol. 2001; 280(4):R1085–1094. [PubMed: 11247831]

Chen Z, Travers SP, Travers JB. Inhibitory modulation of optogenetically identified neuron subtypes in the rostral solitary nucleus. J Neurophysiol. 2016; 116(2):391–403. DOI: 10.1152/jn.00168.2016 [PubMed: 27146980]

Contreras RJ, Beckstead RM, Norgren R. The central projections of the trigeminal, facial, glossopharyngeal and vagus nerves: an autoradiographic study in the rat. J Auton Nerv Syst. 1982; 6(3):303–322. [PubMed: 7169500]

Contreras RJ, Gomez MM, Norgren R. Central origins of cranial nerve parasympathetic neurons in the rat. J Comp Neurol. 1980; 190(2):373–394. [PubMed: 7381063]

Corson JA, Aldridge A, Wilmoth K, Erisir A. A survey of oral cavity afferents in the rat nucleus tractus solitarii. J. Comp Neurol. 2012; 520(3):495–527. [PubMed: 21800298]

Corson JA, Bradley RM. Physiological and anatomical properties of intramedullary projection neurons in rat rostral nucleus of the solitary tract. J Neurophysiol. 2013; 110(5):1130–1143. [PubMed: 23741045]

Danielsen EH, Magnuson DJ, Gray TS. The central amygdaloid nucleus innervation of the dorsal vagal complex in rat: a Phaseolus vulgaris leucoagglutinin lectin anterograde tracing study. Brain Res Bull. 1989; 22(4):705–715. [PubMed: 2736396]

Davis JD, Perez MC. Food deprivation- and palatability-induced microstructural changes in ingestive behavior. Am J Physiol. 1993; 264(1 Pt 2):R97–103. [PubMed: 8430892]

Davis JD, Smith GP, Singh B. Type of negative feedback controlling sucrose ingestion depends on sucrose concentration. Am J Physiol Regul Integr Comp Physiol. 2000; 278(2):R383–389. [PubMed: 10666139]

de Araujo IE, Geha P, Small DM. Orosensory and Homeostatic Functions of the Insular Taste Cortex. Chemosens Percept. 2012; 5(1):64–79. DOI: 10.1007/s12078-012-9117-9 [PubMed: 25485032]

Edwards IJ, Deuchars SA, Deuchars J. The intermedius nucleus of the medulla: a potential site for the integration of cervical information and the generation of autonomic responses. J Chem Neuroanat. 2009; 38(3):166–175. [PubMed: 19790285]

Fallon JH, Leslie FM. Distribution of dynorphin and enkephalin peptides in the rat brain. J Comp Neurol. 1986; 249(3):293–336. [PubMed: 2874159]

Finger TE, Danilova V, Barrows J, Bartel DL, Vigers AJ, Stone L, Kinnamon SC. ATP signaling is crucial for communication from taste buds to gustatory nerves. Science. 2005; 310(5753):1495–1499. [PubMed: 16322458]

Flynn FW, Grill HJ. Insulin elicits ingestion in decerebrate rats. Science. 1983; 221(4606):188–190. [PubMed: 6344221]

Ganchrow D, Ganchrow JR, Cicchini V, Bartel DL, Kaufman D, Girard D, Whitehead MC. Nucleus of the solitary tract in the C57BL/6J mouse: Subnuclear parcellation, chorda tympani nerve projections, and brainstem connections. J Comp Neurol. 2014; 522(7):1565–1596. DOI: 10.1002/cne.23484 [PubMed: 24151133]

Garcia J, Hankins WG, Rusiniak KW. Behavioral regulation of the milieu interne in man and rat. Science. 1974; 185(4154):824–831. [PubMed: 11785521]

Geran LC, Travers SP. Single neurons in the nucleus of the solitary tract respond selectively to bitter taste stimuli. J Neurophysiol. 2006; 96(5):2513–2527. [PubMed: 16899635]

Giza BK, Deems RO, Vanderweele DA, Scott TR. Pancreatic glucagon suppresses gustatory responsiveness to glucose. Am J Physiol. 1993; 265(6 Pt 2):R1231–1237. [PubMed: 8285262]

Giza BK, Scott TR. Blood glucose selectively affects taste-evoked activity in rat nucleus tractus solitarius. Physiol Behav. 1983; 31(5):643–650. [PubMed: 6665054]

Giza BK, Scott TR. Intravenous insulin infusions in rats decrease gustatory-evoked responses to sugars. Am J Physiol. 1987; 252(5 Pt 2):R994–1002. [PubMed: 3555122]

Giza BK, Scott TR, Antonucci RF. Effect of cholecystokinin on taste responsiveness in rats. Am J Physiol. 1990; 258(6 Pt 2):R1371–1379. [PubMed: 2360687]

Giza BK, Scott TR, Vanderweele DA. Administration of satiety factors and gustatory responsiveness in the nucleus tractus solitarius of the rat. Brain Res Bull. 1992; 28(4):637–639. [PubMed: 1617448]

Gjorstrup P. Taste and chewing as stimuli for the secretion of amylase from the parotid gland of the rabbit. Acta Physiol Scand. 1980; 110(3):295–301. [PubMed: 6163322]

Glendinning JI, Frim YG, Hochman A, Lubitz GS, Basile AJ, Sclafani A. Glucose elicits cephalic-phase insulin release in mice by activating KATP channels in taste cells. Am J Physiol Regul Integr Comp Physiol. 2017; 312(4):R597–R610. DOI: 10.1152/ajpregu.00433.2016 [PubMed: 28148491]

Glenn JF, Erickson RP. Gastric modulation of gustatory afferent activity. Physiol Behav. 1976; 16:561–568. [PubMed: 972948]

Grigson PS, Reilly S, Scalera G, Norgren R. The parabrachial nucleus is essential for acquisition of a conditioned odor aversion in rats. Behav Neurosci. 1998; 112(5):1104–1113. [PubMed: 9829788]

Grill HJ, Berridge KC, Ganster DJ. Oral glucose is the prime elicitor of preabsorptive insulin secretion. Am J Physiol. 1984; 246(1 Pt 2):R88–95. [PubMed: 6364839]

Grill HJ, Norgren R. Chronically decerebrate rats demonstrate satiation but not bait shyness. Science. 1978; 201(4352):267–269. [PubMed: 663655]

Grill HJ, Schulkin J, Flynn FW. Sodium homeostasis in chronic decerebrate rats. Behav Neurosci. 1986; 100(4):536–543. [PubMed: 3741604]

Gwyn DG, Leslie RA, Hopkins DA. Observations on the afferent and efferent organization of the vagus nerve and the innervation of the stomach in the squirrel monkey. J Comp Neurol. 1985; 239(2):163–175. DOI: 10.1002/cne.902390204 [PubMed: 4044932]

Hajnal A, Takenouchi K, Norgren R. Effect of intraduodenal lipid on parabrachial gustatory coding in awake rats. J Neurosci. 1999; 19(16):7182–7190. [PubMed: 10436071]

Halsell CB. Differential distribution of amygdaloid input across rostral solitary nucleus subdivisions in rat. Ann N Y Acad Sci. 1998; 855:482–485. [PubMed: 9929642]

Halsell CB, Travers SP, Travers JB. Ascending and descending projections from the rostral nucleus of the solitary tract originate from separate neuronal populations. Neuroscience. 1996; 72(1):185–197. [PubMed: 8730716]

Hamilton RB, Norgren R. Central projections of gustatory nerves in the rat. J Comp Neurol. 1984; 222(4):560–577. [PubMed: 6199385]

Harrison TA, Hoover DB, King MS. Distinct regional distributions of NK1 and NK3 neurokinin receptor immunoreactivity in rat brainstem gustatory centers. Brain Res Bull. 2004; 63(1):7–17. [PubMed: 15121234]

Hayama T, Ogawa H. Two loci of the insular cortex project to the taste zone of the nucleus of the solitary tract in rats. Neurosci Lett. 2001; 303(1):49–52. [PubMed: 11297821]

Herbert H, Moga MM, Saper CB. Connections of the parabrachial nucleus with the nucleus of the solitary tract and the medullary reticular formation in the rat. J Comp Neurol. 1990; 293(4):540–580. [PubMed: 1691748]

Hermann GE, Kohlerman NJ, Rogers RC. Hepatic-vagal and gustatory afferent interactions in the brainstem of the rat. J Auton Nerv Syst. 1983; 9(2–3):477–495. [PubMed: 6363505]

Hermann GE, Rogers RC. Convergence of vagal and gustatory afferent input within the parabrachial nucleus of the rat. J Auton Nerv Syst. 1985; 13(1):1–17. [PubMed: 3998395]

Hockman CH, Hagstrom EC, Hoff EC. Salivary Response to Stimulation of Gastric Branches of Vagus Nerve. Am J Physiol. 1965; 209:119–121. [PubMed: 14343746]

Hu HH, Travers JB, Travers S. Subnuclear location of orosensory neurons in the nucleus of the solitary tract. Society for Neuroscience Abstracts. 1997; 23:1036.

Inui-Yamamoto C, Yuichi F, Takashi Y. Hedonics of taste influence the gastric emptying in rats. Physiol Behav. 2009; 96(4–5):717–722. DOI: 10.1016/j.physbeh.2009.01.013 [PubMed: 19385026]

Kalia M, Fuxe K, Goldstein M. Rat medulla oblongata. II. Dopaminergic, noradrenergic (A1 and A2) and adrenergic neurons, nerve fibers, and presumptive terminal processes. J Comp Neurol. 1985a; 233(3):308–332. DOI: 10.1002/cne.902330303 [PubMed: 2858497]

Kalia M, Fuxe K, Goldstein M. Rat medulla oblongata. III. Adrenergic (C1 and C2) neurons, nerve fibers and presumptive terminal processes. J Comp Neurol. 1985b; 233(3):333–349. DOI: 10.1002/cne.902330304 [PubMed: 2858498]

Kang BJ, Chang DA, Mackay DD, West GH, Moreira TS, Takakura AC, Stornetta RL. Central nervous system distribution of the transcription factor Phox2b in the adult rat. J Comp Neurol. 2007; 503(5):627–641. DOI: 10.1002/cne.21409 [PubMed: 17559094]

Kaplan JM, Seeley RJ, Grill HJ. Daily caloric intake in intact and chronic decerebrate rats. Behav Neurosci. 1993; 107(5):876–881. [PubMed: 8280397]

Karimnamazi H, Travers SP, Travers JB. Oral and gastric input to the parabrachial nucleus of the rat. Brain Res. 2002; 957(2):193–206. [PubMed: 12445962]

Kawamura Y, Yamamoto T. Studies on neural mechanisms of the gustatory-salivary reflex in rabbits. J Physiol. 1978; 285:35–47. [PubMed: 745092]

Kim M, Chiego DJ Jr, Bradley RM. Morphology of parasympathetic neurons innervating rat lingual salivary glands. Auton Neurosci. 2004; 111(1):27–36. DOI: 10.1016/j.autneu.2004.01.006 [PubMed: 15109936]

Kinzeler NR. Circuitry and Function of Mu Opioid Ligands in the Rostral Nucleus of the Solitary Tract and Reticular Formation. (PhD). Ohio State University; Columbus Ohio: 2011.

Kinzeler NR, Travers SP. Mu opiates infused into the NST significantly alter fluid-induced licking and gaping; Paper presented at the International Symposium on Olfaction and Taste; San Francisco, CA. 2008.

Kotz CM, Billington CJ, Levine AS. Opioids in the nucleus of the solitary tract are involved in feeding in the rat. Am J Physiol. 1997; 272(4 Pt 2):R1028–1032. [PubMed: 9139997]

Kreisler AD, Davis EA, Rinaman L. Differential activation of chemically identified neurons in the caudal nucleus of the solitary tract in non-entrained rats after intake of satiating vs. non-satiating meals. Physiol Behav. 2014; 136:47–54. DOI: 10.1016/j.physbeh.2014.01.015 [PubMed: 24508750]

Maier JX. Single-neuron responses to intraoral delivery of odor solutions in primary olfactory and gustatory cortex. J Neurophysiol. 2017; 117(3):1293–1304. DOI: 10.1152/jn.00802.2016 [PubMed: 28003413]

Matsuo R, Yamauchi Y, Kobashi M, Funahashi M, Mitoh Y, Adachi A. Role of parabrachial nucleus in submandibular salivary secretion induced by bitter taste stimulation in rats. Auton Neurosci. 2001; 88(1–2):61–73. [PubMed: 11474548]

McPheeters M, Hettinger TP, Nuding SC, Savoy LD, Whitehead MC, Frank ME. Taste-responsive neurons and their locations in the solitary nucleus of the hamster. Neuroscience. 1990; 34(3):745–758. [PubMed: 2352650]

Norgren R. Taste pathways to hypothalamus and amygdala. J Comp Neurol. 1976; 166(1):17–30. [PubMed: 1262547]

Norgren R, Pfaffmann C. The pontine taste area in the rat. Brain Res. 1975; 91(1):99–117. [PubMed: 1131704]

Norgren R, Smith GP. Central distribution of subdiaphragmatic vagal branches in the rat. J Comp Neurol. 1988; 273(2):207–223. [PubMed: 3417902]

Okada T, Tashiro Y, Kato F, Yanagawa Y, Obata K, Kawai Y. Quantitative and immunohistochemical analysis of neuronal types in the mouse caudal nucleus tractus solitarius: focus on GABAergic neurons. J Chem Neuroanat. 2008; 35(3):275–284. DOI: 10.1016/j.jchemneu.2008.02.001 [PubMed: 18359605]

Pattyn A, Morin X, Cremer H, Goridis C, Brunet JF. Expression and interactions of the two closely related homeobox genes Phox2a and Phox2b during neurogenesis. Development. 1997; 124(20): 4065–4075. [PubMed: 9374403]

Reilly S, Bornovalova MA. Conditioned taste aversion and amygdala lesions in the rat: a critical review. Neurosci Biobehav Rev. 2005; 29(7):1067–1088. DOI: 10.1016/j.neubiorev.2005.03.025 [PubMed: 15893375]

Reilly S, Grigson PS, Norgren R. Parabrachial nucleus lesions and conditioned taste aversion: evidence supporting an associative deficit. Behav Neurosci. 1993; 107(6):1005–1017. [PubMed: 8136054]

Riley CA, King MS. Differential effects of electrical stimulation of the central amygdala and lateral hypothalamus on fos-immunoreactive neurons in the gustatory brainstem and taste reactivity behaviors in conscious rats. Chem Senses. 2013; 38(8):705–717. DOI: 10.1093/chemse/bjt039 [PubMed: 23978688]

Rinaman L. Hindbrain noradrenergic lesions attenuate anorexia and alter central cFos expression in rats after gastric viscerosensory stimulation. J Neurosci. 2003; 23(31):10084–10092. [PubMed: 14602823]

Rinaman L. Ascending projections from the caudal visceral nucleus of the solitary tract to brain regions involved in food intake and energy expenditure. Brain Res. 2010; 1350:18–34. [PubMed: 20353764]

Rinaman L. Hindbrain noradrenergic A2 neurons: diverse roles in autonomic, endocrine, cognitive, and behavioral functions. Am J Physiol Regul Integr Comp Physiol. 2011; 300(2):R222–235. [PubMed: 20962208]

Ross CA, Ruggiero DA, Reis DJ. Projections from the nucleus tractus solitarii to the rostral ventrolateral medulla. J Comp Neurol. 1985; 242(4):511–534. [PubMed: 2418079]

Samuelsen CL, Fontanini A. Processing of Intraoral Olfactory and Gustatory Signals in the Gustatory Cortex of Awake Rats. J Neurosci. 2017; 37(2):244–257. DOI: 10.1523/JNEUROSCI.1926-16.2016 [PubMed: 28077705]

Scalera G, Spector AC, Norgren R. Excitotoxic lesions of the parabrachial nuclei prevent conditioned taste aversions and sodium appetite in rats. Behav Neurosci. 1995; 109(5):997–1008. [PubMed: 8554723]

Schier LA, Davidson TL, Powley TL. Ongoing ingestive behavior is rapidly suppressed by a preabsorptive, intestinal "bitter taste" cue. Am J Physiol Regul Integr Comp Physiol. 2011; 301(5):R1557–1568. DOI: 10.1152/ajpregu.00344.2011 [PubMed: 21865540]

Schier LA, Spector AC. Post-oral sugar detection rapidly and chemospecifically modulates taste-guided behavior. Am J Physiol Regul Integr Comp Physiol. 2016; 311(4):R742–R755. DOI: 10.1152/ajpregu.00155.2016 [PubMed: 27511277]

Schmued L, Slikker W Jr. Black-gold: a simple, high resolution histochemical label for normal and pathological myelin in brain tissue sections. Brain Res. 1999; 837(1–2):289–297. [PubMed: 10434014]

Sclafani A. Gut-brain nutrient signaling. Appetition vs. satiation. Appetite. 2013; 71:454–458. DOI: 10.1016/j.appet.2012.05.024 [PubMed: 22664300]

Seeley RJ, Grill HJ, Kaplan JM. Neurological dissociation of gastrointestinal and metabolic contributions to meal size control. Behav Neurosci. 1994; 108(2):347–352. [PubMed: 8037879]

Shapiro RE, Miselis RR. The central organization of the vagus nerve innervating the stomach of the rat. J Comp Neurol. 1985; 238(4):473–488. DOI: 10.1002/cne.902380411 [PubMed: 3840183]

Spector AC, Klumpp PA, Kaplan JM. Analytical issues in the evaluation of food deprivation and sucrose concentration effects on the microstructure of licking behavior in the rat. Behav Neurosci. 1998; 112(3):678–694. [PubMed: 9676983]

Spector AC, le Roux CW, Munger SD, Travers SP, Sclafani A, Mennella JA. Proceedings of the 2015 A.S.P.E.N. Research Workshop-Taste Signaling: Impact on Food Selection, Intake, and Health. JPEN J Parenter Enteral Nutr. 2015; doi: 10.1177/0148607115617438

Spector AC, Travers SP. The representation of taste quality in the mammalian nervous system. Behav Cogn Neurosci Rev. 2005; 4(3):143–191. [PubMed: 16510892]

Stanley BG, Kyrkouli SE, Lampert S, Leibowitz SF. Neuropeptide Y chronically injected into the hypothalamus: a powerful neurochemical inducer of hyperphagia and obesity. Peptides. 1986; 7(6):1189–1192. [PubMed: 3470711]

Stornetta RL, Guyenet PG. Distribution of glutamic acid decarboxylase mRNA-containing neurons in rat medulla projecting to thoracic spinal cord in relation to monoaminergic brainstem neurons. J Comp Neurol. 1999; 407(3):367–380. [PubMed: 10320217]

Stornetta RL, Sevigny CP, Guyenet PG. Vesicular glutamate transporter DNPI/VGLUT2 mRNA is present in C1 and several other groups of brainstem catecholaminergic neurons. J Comp Neurol. 2002; 444(3):191–206. [PubMed: 11840474]

Stratford JM, Thompson JA, Finger TE. Immunocytochemical organization and sour taste activation in the rostral nucleus of the solitary tract of mice. J Comp Neurol. 2016; doi: 10.1002/cne.24059

Tamamaki N, Yanagawa Y, Tomioka R, Miyazaki J, Obata K, Kaneko T. Green fluorescent protein expression and colocalization with calretinin, parvalbumin, and somatostatin in the GAD67-GFP knock-in mouse. J Comp Neurol. 2003; 467(1):60–79. [PubMed: 14574680]

Taylor K, Lester E, Hudson B, Ritter S. Hypothalamic and hindbrain NPY, AGRP and NE increase consummatory feeding responses. Physiol Behav. 2007; 90(5):744–750. [PubMed: 17289093]

Travagli RA, Hermann GE, Browning KN, Rogers RC. Brainstem circuits regulating gastric function. Annu Rev Physiol. 2006; 68:279–305. [PubMed: 16460274]

Travers SP, Norgren R. Organization of orosensory responses in the nucleus of the solitary tract of rat. J Neurophysiol. 1995; 73(6):2144–2162. [PubMed: 7666129]

Ueda H, Suga M, Yagi T, Kusumoto-Yoshida I, Kashiwadani H, Kuwaki T, Miyawaki S. Vagal afferent activation induces salivation and swallowing-like events in anesthetized rats. Am J Physiol Regul Integr Comp Physiol. 2016; 311(5):R964–R970. DOI: 10.1152/ajpregu.00292.2016 [PubMed: 27707722]

van der Kooy D, Koda LY, McGinty JF, Gerfen CR, Bloom FE. The organization of projections from the cortex, amygdala, and hypothalamus to the nucleus of the solitary tract in rat. J Comp Neurol. 1984; 224(1):1–24. [PubMed: 6715573]

Vandenbeuch A, Larson ED, Anderson CB, Smith SA, Ford AP, Finger TE, Kinnamon SC. Postsynaptic P2×3-containing receptors in gustatory nerve fibres mediate responses to all taste qualities in mice. J Physiol. 2015; 593(5):1113–1125. DOI: 10.1113/jphysiol.2014.281014 [PubMed: 25524179]

Wang M, Bradley RM. Properties of GABAergic neurons in the rostral solitary tract nucleus in mice. J Neurophysiol. 2010; 103(6):3205–3218. [PubMed: 20375246]

Wang Y, Kakizaki T, Sakagami H, Saito K, Ebihara S, Kato M, Yanagawa Y. Fluorescent labeling of both GABAergic and glycinergic neurons in vesicular GABA transporter (VGAT)-venus transgenic mouse. Neuroscience. 2009; 164(3):1031–1043. [PubMed: 19766173]

Warlow SM, Robinson MJF, Berridge KC. Optogenetic Central Amygdala Stimulation Intensifies and Narrows Motivation for Cocaine. J Neurosci. 2017; 37(35):8330–8348. DOI: 10.1523/JNEUROSCI.3141-16.2017 [PubMed: 28751460]

Whitehead MC. Anatomy of the gustatory system in the hamster: synaptology of facial afferent terminals in the solitary nucleus. J Comp Neurol. 1986; 244(1):72–85. [PubMed: 3950091]

Whitehead MC. Neuronal architecture of the nucleus of the solitary tract in the hamster. J Comp Neurol. 1988; 276(4):547–572. [PubMed: 2461969]

Whitehead MC. Subdivisions and neuron types of the nucleus of the solitary tract that project to the parabrachial nucleus in the hamster. J Comp Neurol. 1990; 301(4):554–574. [PubMed: 2177063]

Whitehead MC. Distribution of synapses on identified cell types in a gustatory subdivision of the nucleus of the solitary tract. J Comp Neurol. 1993; 332(3):326–340. [PubMed: 8331219]

Whitehead MC, Bergula A, Holliday K. Forebrain projections to the rostral nucleus of the solitary tract in the hamster. J Comp Neurol. 2000; 422(3):429–447. [PubMed: 10861518]

Wicks D, Wright J, Rayment P, Spiller R. Impact of bitter taste on gastric motility. Eur J Gastroenterol Hepatol. 2005; 17(9):961–965. [PubMed: 16093874]

Williams EK, Chang RB, Strochlic DE, Umans BD, Lowell BB, Liberles SD. Sensory Neurons that Detect Stretch and Nutrients in the Digestive System. Cell. 2016; 166(1):209–221. DOI: 10.1016/j.cell.2016.05.011 [PubMed: 27238020]

Yokota T, Eguchi K, Hiraba K. Topographical representations of taste response characteristics in the rostral nucleus of the solitary tract in the rat. J Neurophysiol. 2014; 111(1):182–196. DOI: 10.1152/jn.01031.2012 [PubMed: 24133228]

Zaidi FN, Todd K, Enquist L, Whitehead MC. Types of taste circuits synaptically linked to a few geniculate ganglion neurons. J Comp Neurol. 2008; 511(6):753–772. DOI: 10.1002/cne.21869 [PubMed: 18925565]

Zerari-Mailly F, Buisseret P, Buisseret-Delmas C, Nosjean A. Trigemino-solitarii-facial pathway in rats. J Comp Neurol. 2005; 487(2):176–189. [PubMed: 15880487]

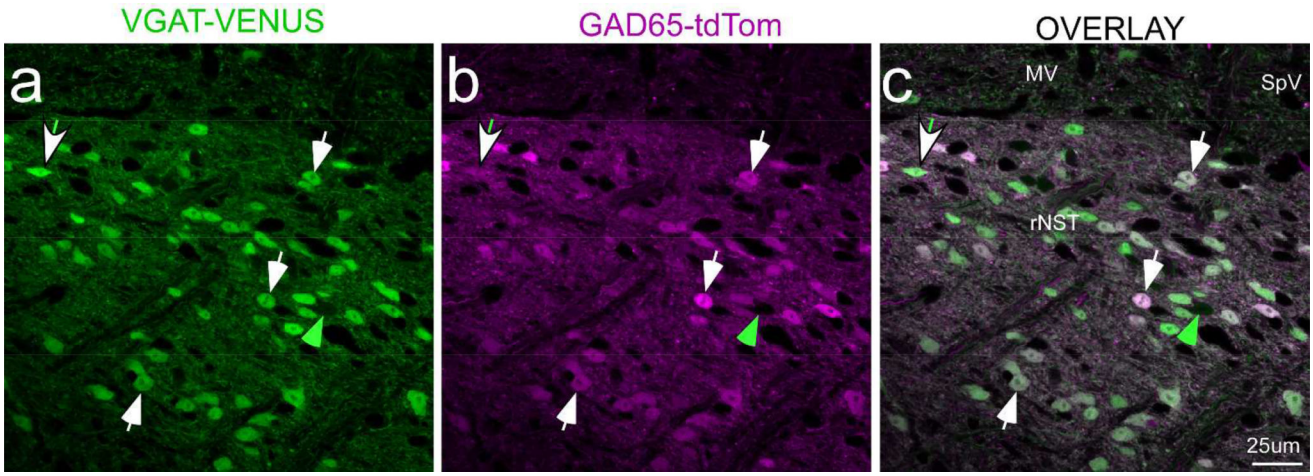

Figure 1.

Confocal micrographs (single Z level) of an rNST section from a mouse that was a cross between a GAD65-tdTom VGAT-Venus mouse. This section was approximately half-way between the rostral pole of the nucleus and the level at which the NST merges with the IVth ventricle. The photo centered on the regions of the rostral central and ventral subdivisions. White arrows illustrate examples of doubly-labeled neurons that were approximately equally bright for Venus and td-Tom; the green arrow denotes a singly-labeled VGAT neuron. The arrow with the white head and green tail points to a doubly-labeled neuron with more intense Venus than td-Tom label; examples of the converse were also observed, though none is obvious at this Z level. Scale = 25μm. (Abbreviations- MV: medial vestibular nucleus, rNST: rostral NST, SpV: spinal vestibular nucleus.

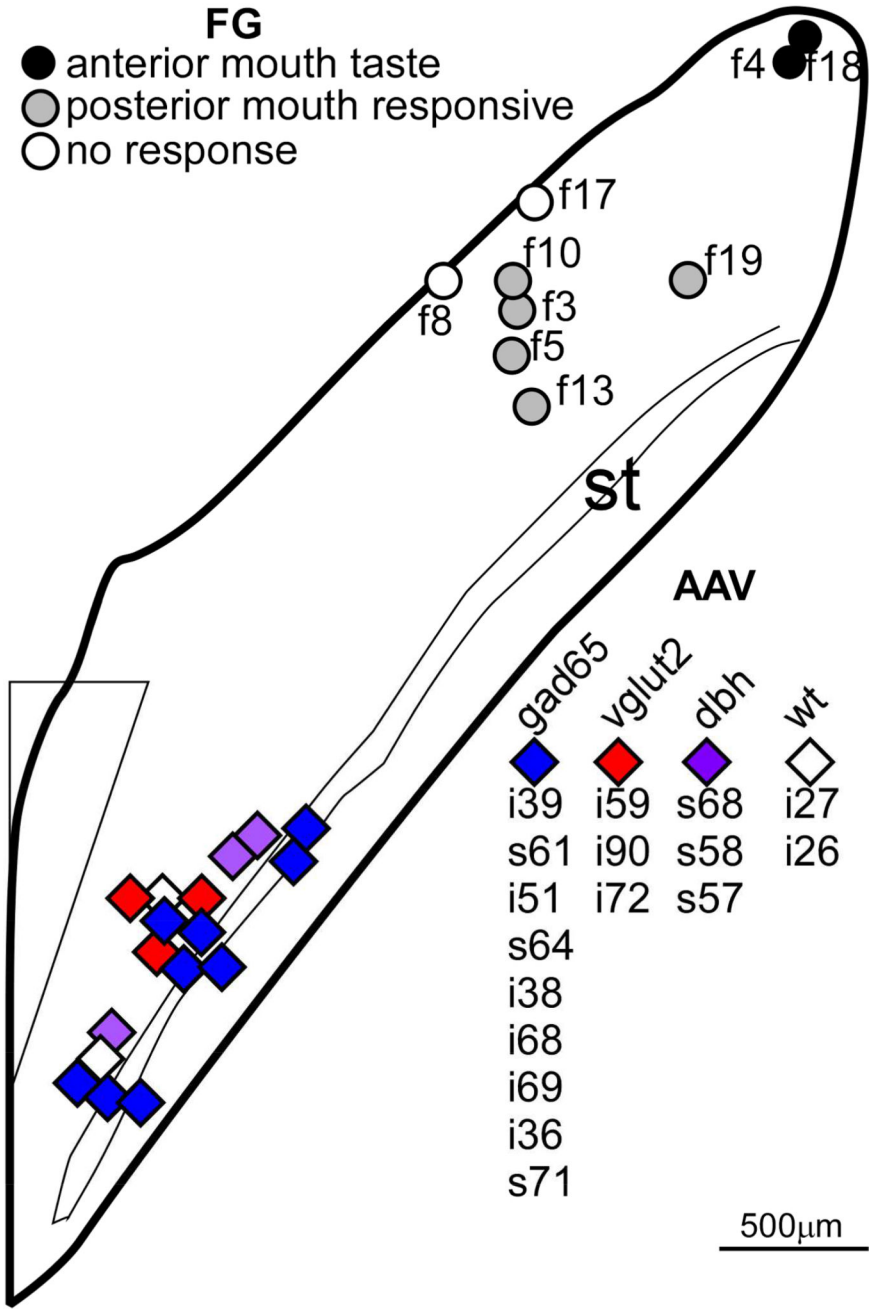

Figure 2.

Horizontal schematic of the NST depicting the locations of the centers of all of the injection sites for the retrograde tracing from the rNST (FG: Fluorogold) and anterograde tracing from the cNST with various AAV viruses. Symbols for Fluorogold injections are coded according to the sensory response recorded through the injection pipette; those for the AAV injections by the strain of mouse either cre-expressing (GAD65, vglut2, dbh) or wild-type (wt). The symbol key is ordered by rostral-caudal location. The schematic is based upon that which appeared Figure 1 in Breza & Travers, 2016, but extends that diagram caudally. Abbreviations- AP: area postrema, st: solitary tract.

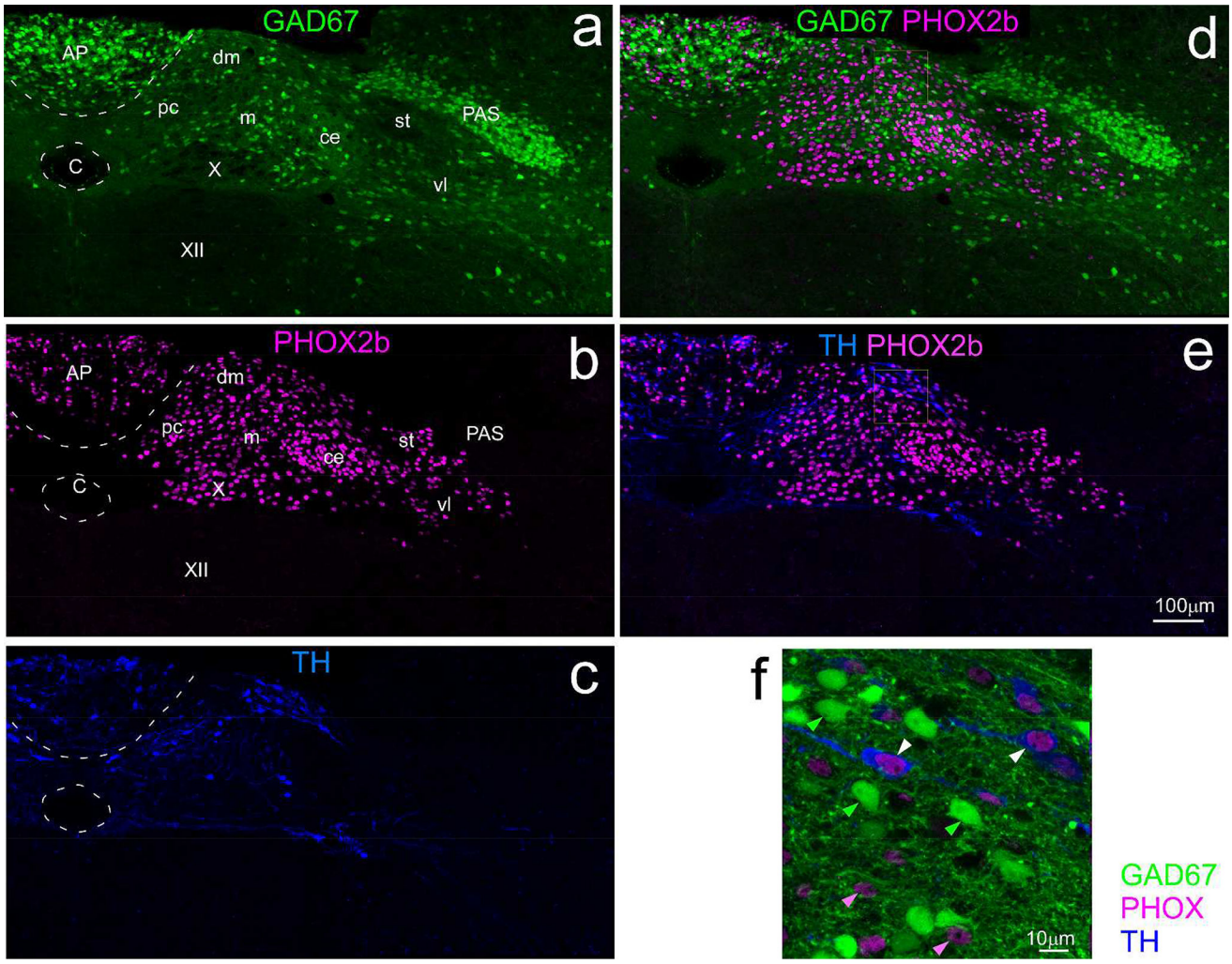

Figure 3.

Confocal photomicrographs of the cNST at the level of the area postrema from a mouse expressing EGFP under the control of the GAD67 promoter (GAD67-EGFP+ mouse). Sections were immunostained for PHOX2b and tyrosine hydroxylase (TH). **Left panels (a,b,c)** show maximum intensity projections (2μm intervals) of single channels for each phenotype, a: GAD67, **b:** PHOX2b, **c:** TH; the two panels on the **upper right (d,e)** show overlap of GAD67 with with PHOX2b **(d)** and TH with PHOX2b **(e)**. Relative to the dense distribution of PHOX2b and TH neurons, GAD67 neurons are sparse near the dorsomedial and parvicellular subnuclei, and denser ventrolaterally in the lateral part of the medial, central, and ventrolateral subnuclei. The panel on the **lower right (f)** is a higher magnification image (maximum intensity projection, four sections, 1μm intervals,) demonstrating that PHOX2b and GAD67 are mutually exclusive markers, whereas TH is co-expressed in a subset of PHOX2b neurons; note that PHOX2b is localized to nuclei, whereas the other markers fill the soma. Examples of single-labeled PHOX2b and GAD67 neurons are denoted by the solid pink and green arrowheads; double-labeled PHOX2b+/TH neurons by the white arrowheads. (Abbreviations- AP: area postrema, C: central canal, PAS: parasolitary nucleus, st: solitary tract, X: dorsal motor nucleus of the vagus, XII: hypoglossal

nucleus, subnuclei of the cNST- ce: central, dm: dorsomedial, m: medial, pc: parvicellular, vl: ventrolateral.

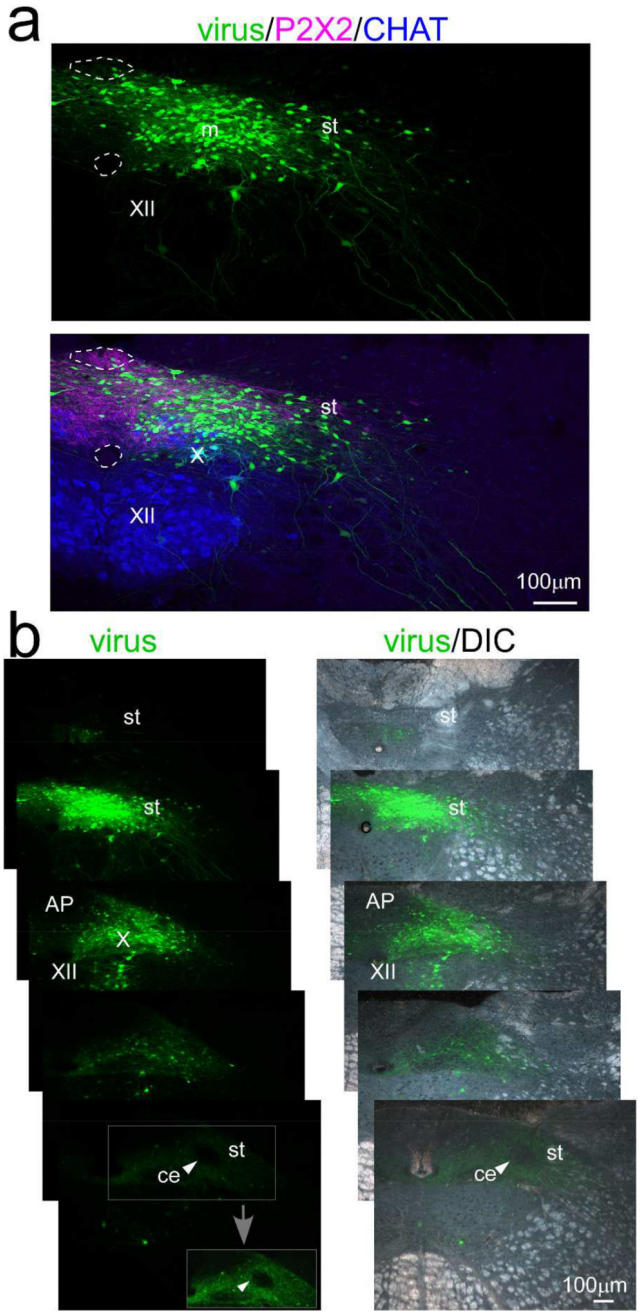

Figure 4.

Injection site for case ISM26 with an injection of an AAV1.hSynap.eGFP virus in cNST centered near the level of obex medial to the solitary tract. **a.** Confocal images near the injection site center. The **upper panel** shows the virus alone and the **lower panel** shows immunostaining for P2×2 which marks the axons and terminals of a subset of primary afferent vagal neurons, and choline acetyltransferase (CHAT), which stains preganglionic parasympathetic neurons in the dorsal motor nucleus of the vagus and motor neurons in the hypoglossal nucleus. Dotted lines denote the borders of the area postrema and central canal in both panels. **b.** Series of low-power photomicrographs of injection site viral labeling alone

(left) and viral labeling superimposed on darkfield images **(right)** arranged from caudal (top) to rostral (bottom). The second section from the top corresponds to the confocal image in (a). Sections are separated by ~250μm, except for the two most rostral, which are adjacent 40μm sections. Although some labeled neurons are apparent outside NST, virtually all of these are confined to the dorsal motor nucleus of the vagus and hypoglossal nucleus, which only send axons to peripheral targets. The arrowhead in the rostral-most section points to the (caudal/intermediate) central subnucleus, which is virtually devoid of afferent labeling. The boxed region containing the central subnucleus is shown with the brightness and contrast enhanced in the inset (gray arrow). Abbreviations- AP: area postrema, C: central canal, ce: central subdivision, CHAT: choline acetyltransferase, m: medial subdivision, st- solitary tract, X: dorsal motor nucleus of the vagus, XII: hypoglossal nucleus.

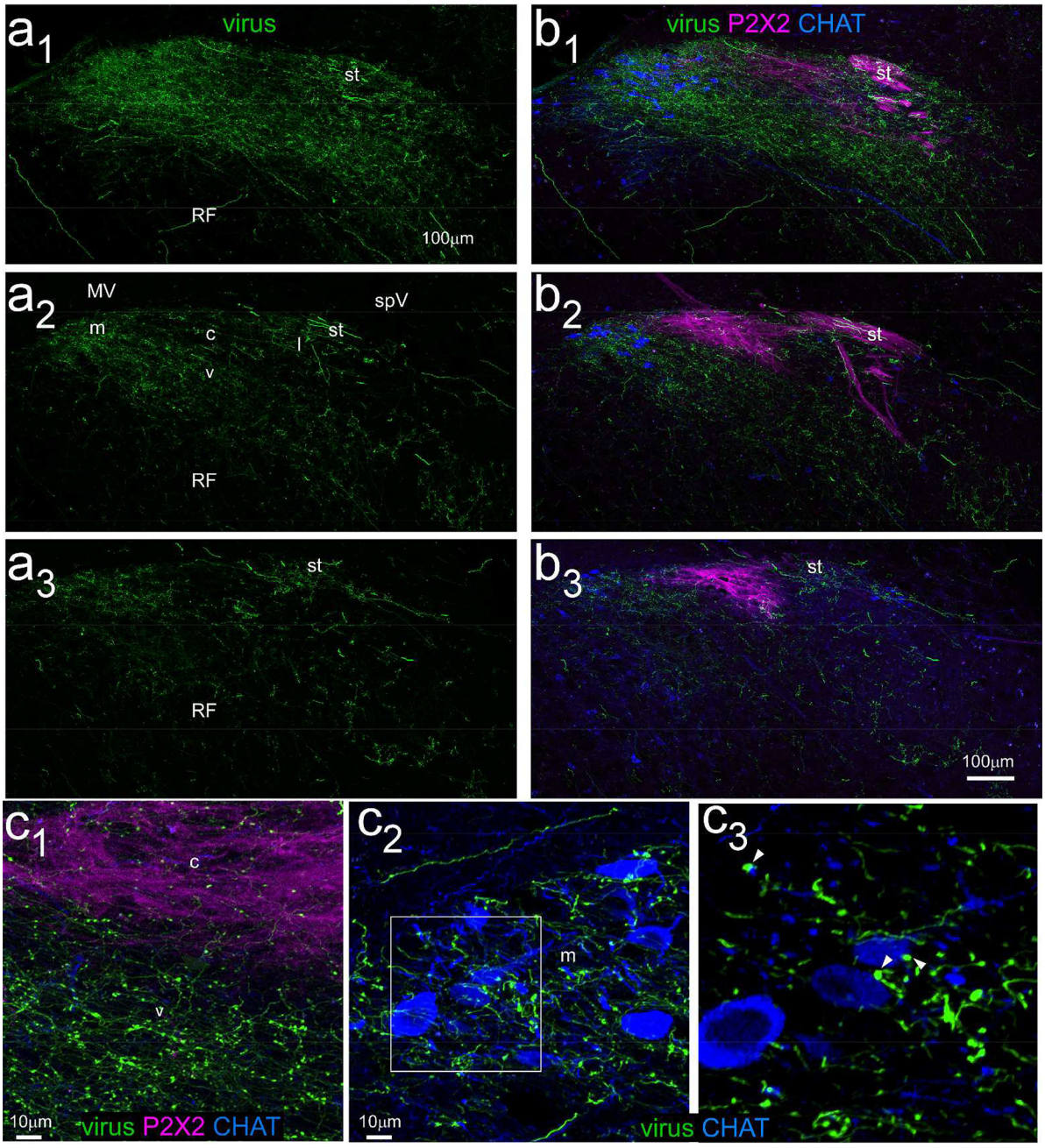

Figure 5.

Confocal photomicrographs (maximum intensity projections, z=2μm intervals) of rNST anterograde labeling arising from the cNST injection shown in Figure 4. **Panels a_1–a_3** depict viral label in three sections arranged from caudal (**a_1**) to rostral (**a_3**). Panel **a_2** is from a mid-level of rNST and denotes the approximate locations of rNST subdivisions. **Panels b_1–b_3** show the same three sections with immunostaining for P2×2 and CHAT. Anterograde labeling is most prominent in the ventral and medial subdivisions, i.e., ventral and medial to the P2×2 field, which largely corresponds to the (rostral) central subdivision. Moreover, the medial projections overlap extensively with CHAT-stained preganglionic parasympathetic

neurons. **Panels c_1–c_3** show high-magnification photomicrographs (maximum intensity projection, z=1um intervals) from a nearby section at the mid-NST level. **C_1:** a field overlapping the P2×2 staining and ventrally adjacent region. Some varicosities are present in the P2×2 field but they are much denser ventrally. **C_2:** medial rNST. Numerous varicosities intermingle with the CHAT neurons. C_3: Magnified image of the area denoted by the white square; this flattened image sed just 9/41 z levels in **C_2**. A few varicosities appear to appose dendrites or somata (arrowheads). Abbreviations- MV: medial vestibular nucleus, SpV: spinal vestibular nucleus, st: solitary tract, RF: reticular formation. rNST subdivisions- m: medial, c: central, v: ventral, l: lateral.

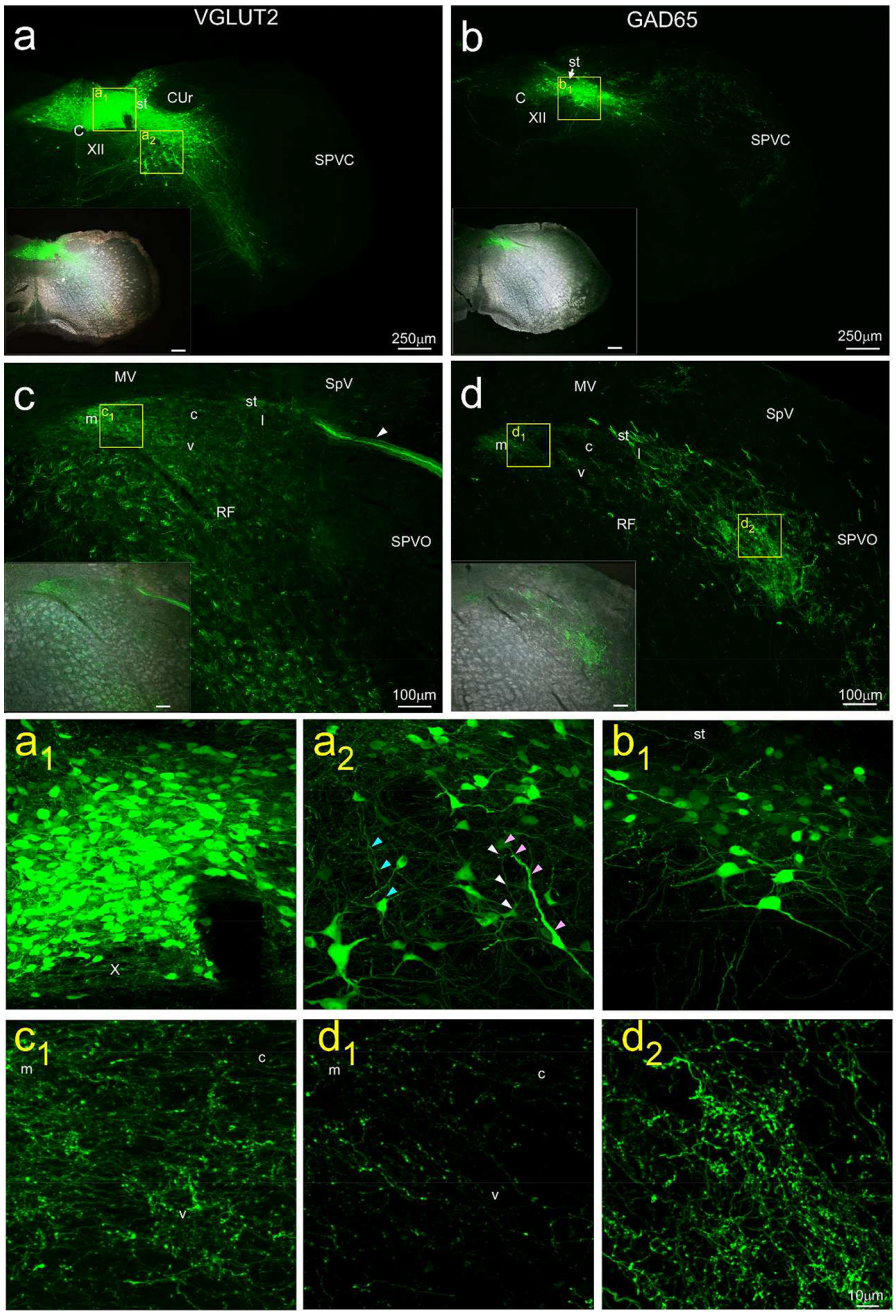

Figure 6.

Caudal NST injection sites (**a & b**) and resulting afferent label in rNST (**c & d**) from injections of a floxed virus (AAV1.CAG.Flex.eGFP.WPRE.bGH) in VGLUT2-cre (**left panels: a & c**, case SL15–58) and GAD65-cre (**right panels: b & d**, case SL15–61) mice. Insets in the lower left portion of each panel show labeling superimposed on darkfield images. The locations of higher-magnification confocal images presented in the lower six panels are denoted by yellow squares. Despite using similar coordinates and injection parameters, the injection site was smaller in the GAD65 case and located more ventrolaterally. Note the lack of labeled cells evident in the hypoglossal nucleus and dorsal

motor nucleus of the vagus for both injections (**a, a$_1$, b**). The injection for the VGLUT2 case included neurons in the intermediate reticular formation (boxed area a$_2$) that had dendrites directed dorsally toward the cNST (**a$_2$**; colored arrows denote dendrites arising from different cells). The patterns of anterograde labeling arising from the VGLUT2 and GAD65 injection sites resembled each other by being more profuse in the medial and ventral rNST than in the central region, albeit overall lighter for the GAD65 case (compare panels **c** and **c1** with **d** and **d$_1$**). The pattern of anterograde labeling for GAD65 was distinctive, however, because it was denser in the lateral subdivision, and extended to the reticular formation and adjacent spinal trigeminal nucleus (panels **d, d$_1$,d$_2$**). The arrowhead in panel (**c**) points to incoming afferent, probably vagal, fibers. Abbreviations- CuR: rotundus division, cuneate nucleus, SpV: spinal vestibular nucleus, MV: medial vestibular nucleus, RF: reticular formation, SPVC: spinal trigeminal nucleus, subnucleus caudalis, SPVO: spinal trigeminal nucleus, subnucleus oralis, st: solitary tract, XII: hypoglossal nucleus. rNST subdivisions- m: medial, c: central, v: ventral, l: lateral.

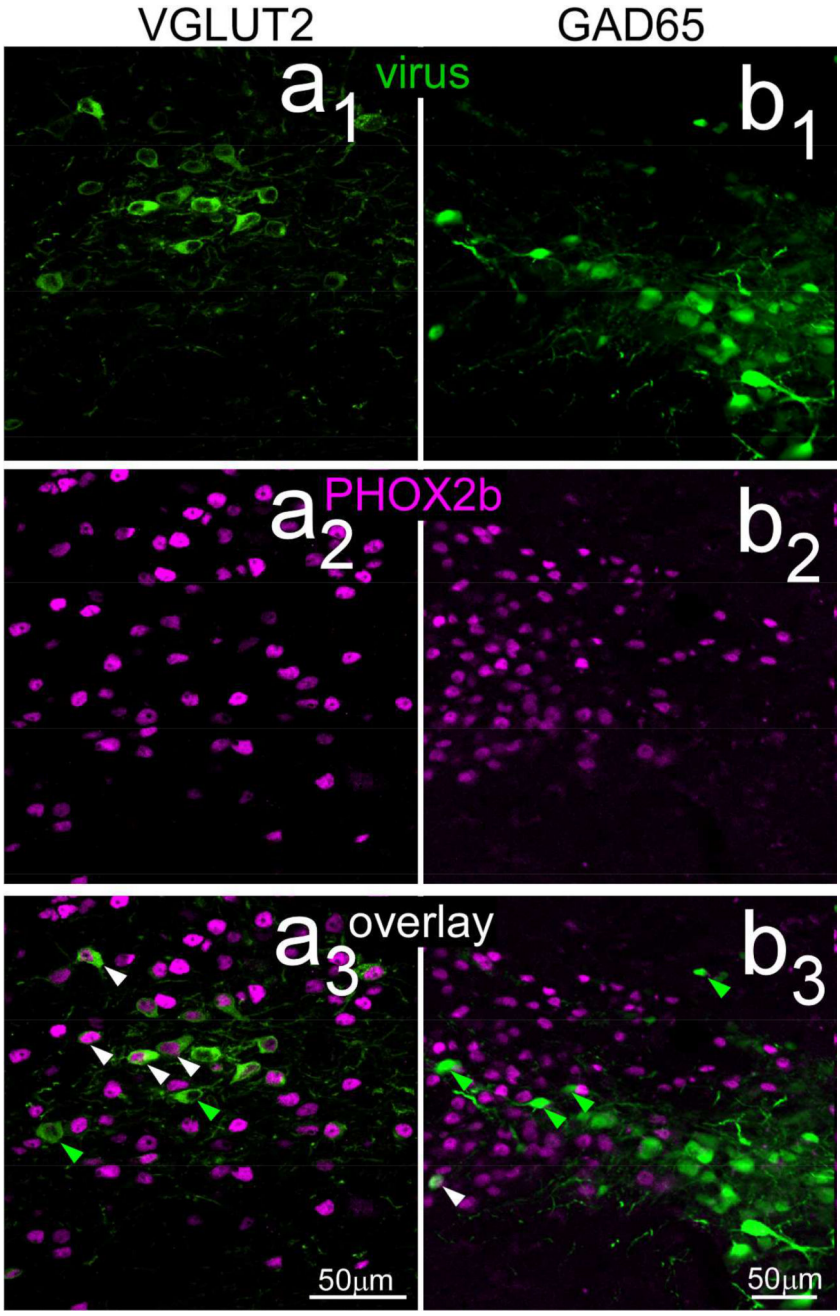

Figure 7.

Confocal photomicrographs (maximum intensity projections, two z levels, z=1μm intervals) near the centers of cre-dependent viral injection sites in VGLUT2 (a1 – a3) and GAD65 (**b_1 – b_3**) therelationship with PHOX2b staining. As described in the text, few virally-labeled neurons in the GAD65-cre mice were double-labeled (**right overlay: b_3**), whereas a majority of those in the VGLUT case were double-labeled (**left overlay: a_3**). Arrowheads show examples of neurons singly-labeled with virus (green) or double-labeled with PHOX2b and virus (white).

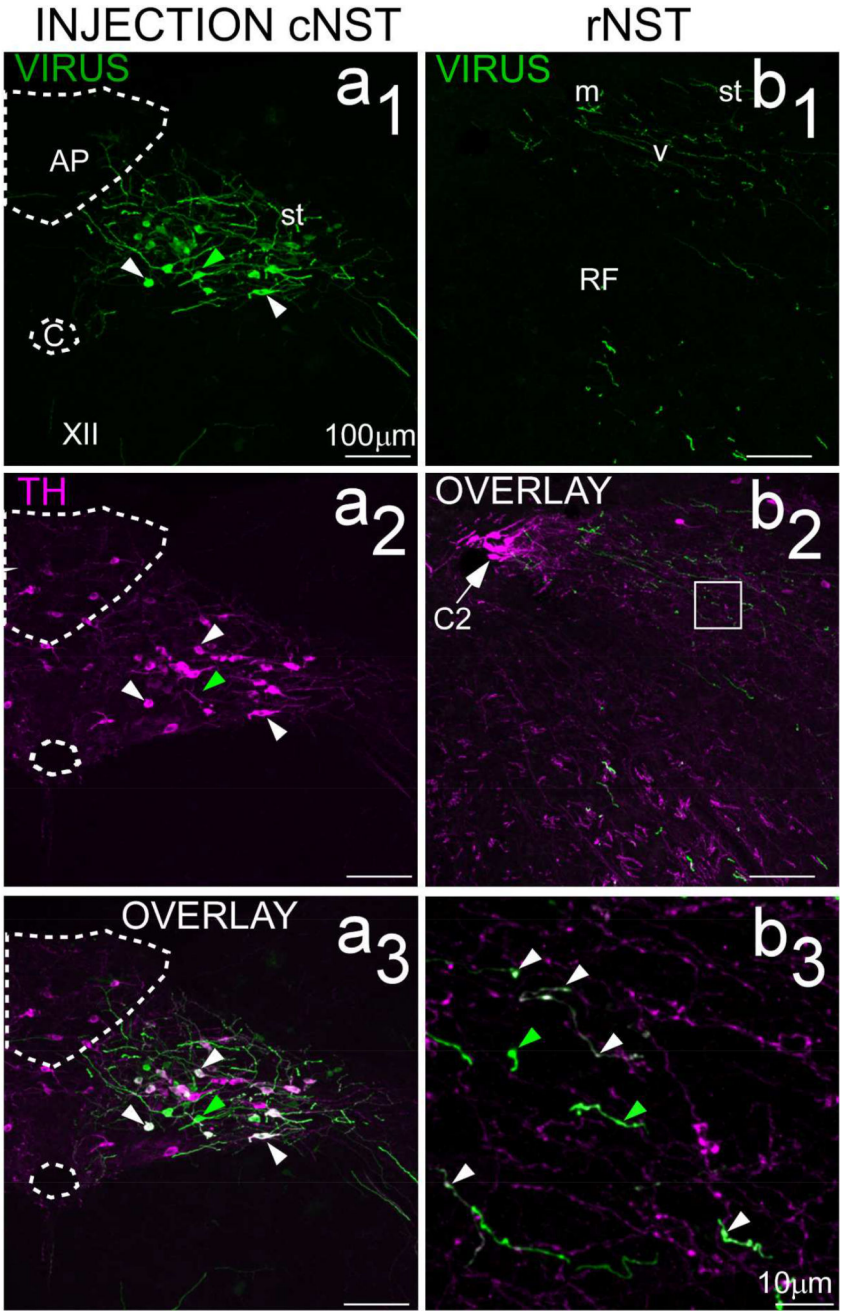

Figure 8.

Confocal images (maximum intensity projections; z=2μm intervals) of the injection site (**left panels: a_1–a_3**) and resulting afferent labeling in rNST (**right panels: b_1 – b_3**) from a DBH-cre mouse receiving an injection of a cre-dependent virus expressing EGFP (AAV1.CAG.Flex.eGFP.WPRE.bGH, case ISM72). As discussed in the text, a majority of neurons intensely labeled with virus were double-labeled for TH (white arrowheads) but some were not (green arrowheads). Afferent labeling in rNST (**b_1 – b_3**) was sparser than for VGLUT or GAD65 projections. **Panel b_3** is a higher magnification of the region indicated by the white square in the lower-magnification image in b_2 (maximum intensity projection,

z=1μm intervals). Fibers singly-labeled for the virus were observed (green arrowheads, **b_3**) but a number of double-labeled fibers with varicosities (white arrowheads) were also evident, supporting the existence of a modest noradrenergic input from cNST. There were also a large number of fibers singly-labeled for TH. Abbreviations- AP: area postrema, C: Central canal, C2: C2 group of catecholaminergic (adrenergic) neurons, st: solitary tract, RF: reticular formation, XII: hypoglossal nucleus.

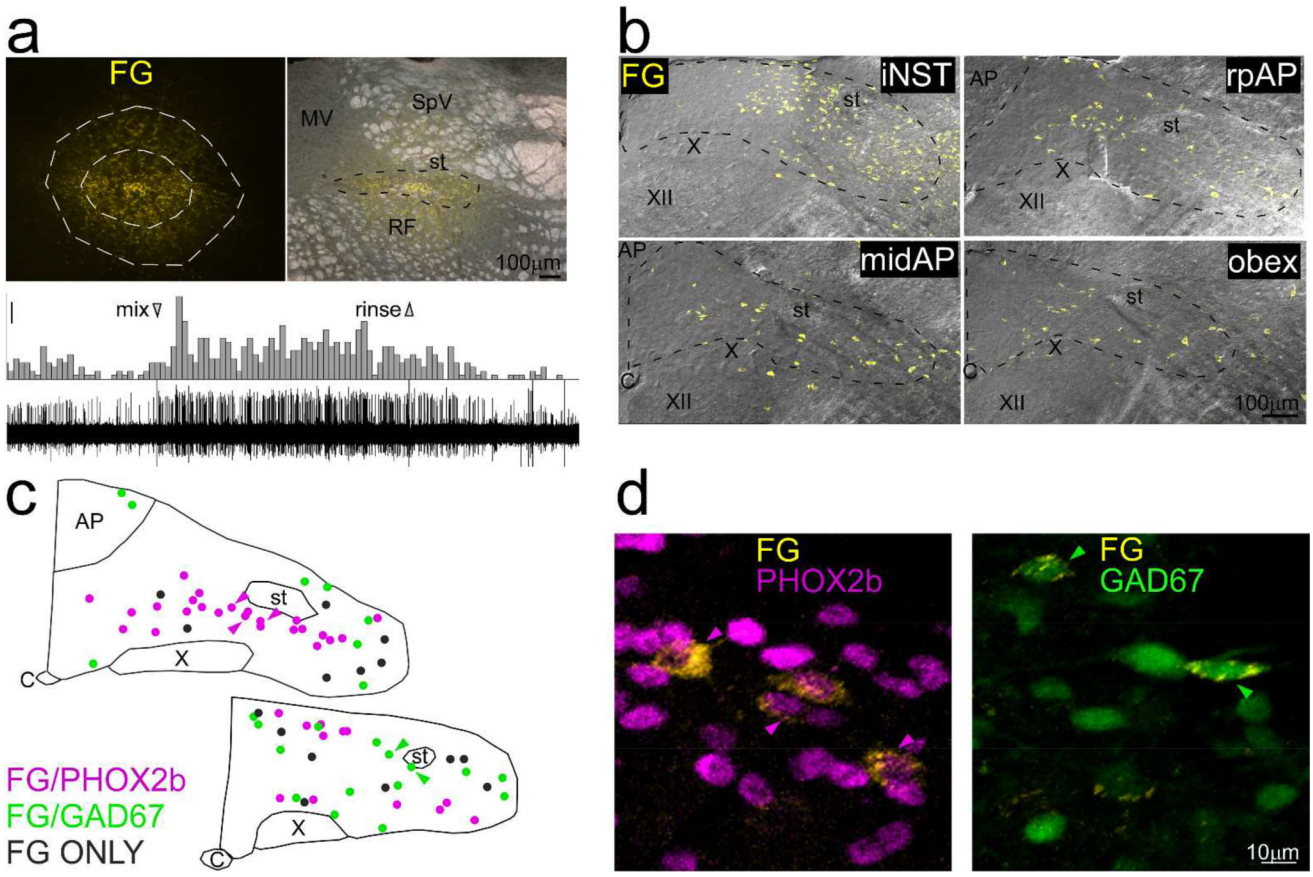

Figure 9.

Example of retrograde tracing in a GAD67-EGFP+ mouse (case ISM4) that received an injection of Fluorogold (FG), near the rostral pole of NST. Fluorogold-labeled neurons are pseudocolored yellow in all panels. **a. Top panels:** Photomicrographs of the injection site. Outlines on the left panel delineate the core (inner outline) and less densely-labeled shell (outer outline) of the injection site; the corresponding measurement appears in figure 10. The right panel shows the injection site superimposed upon a darkfield image of the nucleus. The core was mostly confined to NST, but some labeled cells in the shell extended into the vestibular nucleus dorsally and the reticular formation ventrally. **Lower panel:** Peristimulus-time histogram and raw neural record depicting the multiunit response to a taste mixture applied to the anterior tongue and recorded through the injection pipette. Scale bar for histogram: 5 spikes/500ms. **b.** Maximum intensity projections (2μm intervals) of confocal photomicrographs of retrograde labeling (yellow) superimposed upon corresponding DIC images extending from iNST to a level caudal to obex. **c.** Plots of retrogradely labeled neurons from a mid-level of the AP and obex (from a different series than in **a** and **b**) that was immunostained for PHOX2b. Retrogradely-labeled neurons are color-coded for PHOX2b (pink), GAD67 (green) or retrogradely-labeled only (grey). No neurons, including those retrogradely labeled, were double-labeled for PHOX2b and GAD67. **d.** Higher-magnification photomicrographs of retrogradely-labeled neurons double-labeled for GAD67 or PHOX2b. The arrowheads indicate the same neurons denoted in **c**. Abbreviations- AP: area postrema, C: Central canal, FG: Fluorogold, M: medial vestibular nucleus, RF: reticular

formation, SpV: spinal vestibular nucleus, st: solitary tract, X: dorsal motor nucleus of the vagus, XII: hypoglossal nucleus.

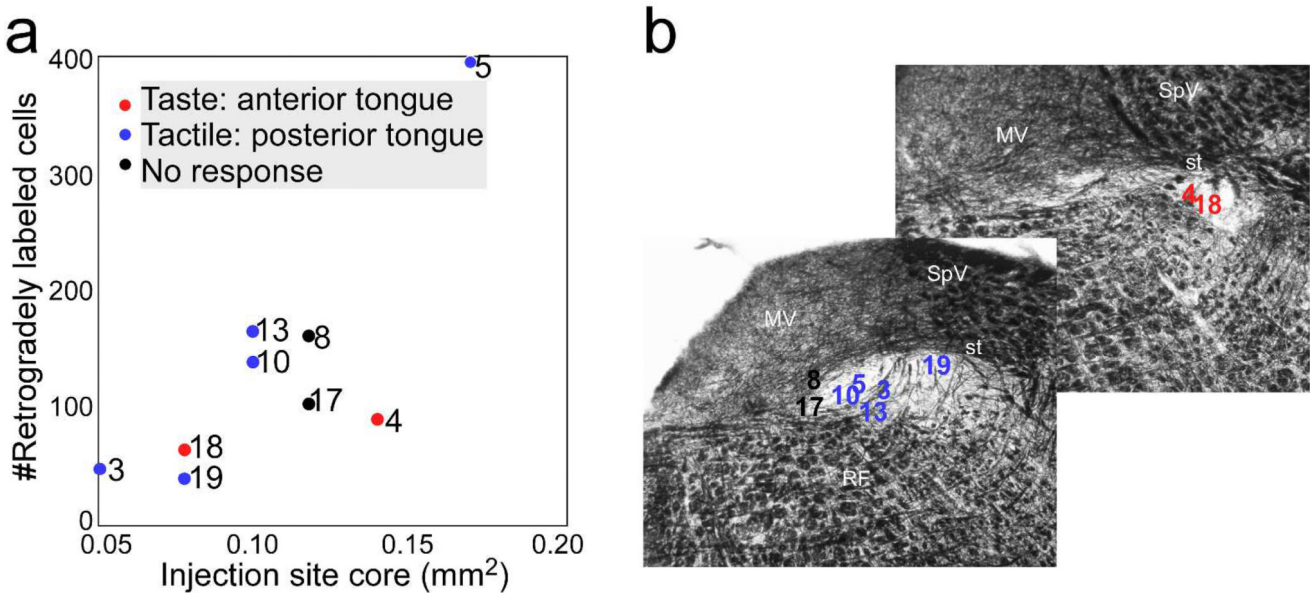

Figure 10.

a. Scatterplot showing the relationship between the size of the injection site and the total number of retrogradely-labeled cells counted at levels of obex and the mid-AP. The numbers indicate the case numbers and the different symbols correspond to the sensory response recorded at the injection. **b.** Approximate locations of the center of each injection site plotted on illustrative rNST sections from a middle level and the rostral pole of rNST stained with black-gold, a stain for myelin. The borders of the NST are highlighted by the relatively light staining in this region, but the solitary tract is intensely stained. Abbreviations- M: medial vestibular nucleus, RF: reticular formation, SpV: spinal vestibular nucleus, st: solitary tract, X: dorsal motor nucleus of the vagus, XII: hypoglossal nucleus.

J Comp Neurol. Author manuscript; available in PMC 2019 October 16.

TABLE 1

ANTEROGRADE VIRUS INJECTIONS[†,‡,§,¶]

Strain nickname	Full Strain Name Source & RRID	N	Mouse ID	Virus Vector (Penn Vector #)	Injection	Survival (d)	Type	Immunohistochemistry
B6	C57BL/6J RRID: ISMR_JAX: 000664	2	ISM36 ISM37	AAV1.CAG.Flex.e GFP.WPRE.bGH (AV-1-ALL854)	4μA/3min	35	Control: cre-dependence of virus	None
GAD67-EGFP−	B6 × GAD67-EGFP+ NEGATIVE OFFSPRING	2	ISM26[†] ISM27	AAV1.hSynap.eGFP.WPRE.bGH (AV1-PV1696)	4μA/3min	18–19	Anterograde: non-specific	P2×2/TH double P2×2/CHAT double
VGLUT2-cre (het)	*Slc17ab*$^{tm2(cre)Lowl}$*/J* (RRID: ISMR_JAX 016963) × C57BL/6J	2	SL15–57 SL15–58[†]	AAV1.CAG.Flex.eGFP.WPRE.bGH (AV-1-ALL854)	10μA/12min	30–36	Anterograde: VGLUT2	P2×2 (SL15–57)
VGLUT2-cre (het)	As above	1	SL15–68[†]	AAV1.CBA.Flex.ChR2 (H134R)-mCherry.WPRES.SV40 AV-1-18916P)	10μA/12min	45	Anterograde: VGLUT2	mCherry PHOX2b
GAD65-cre (hom)	*GAD2*$^{tm2(cre)Zjh}$ */J* RRID: ISMR_JAX: 010802	3 1	SL61[†] SL64 ISM35	AAV1.CAG.Flex.eGFP.WPRE.bGH (AV-1-ALL854)	10μA/12min 4μA/min	32–34 21	Anterograde: GAD65	PHOX2b (ISM61&64) P2×2 (ISM64)
GAD65-cre (het)	*GAD2*$^{tm2(cre)Zjh}$*/J* × C57BL/6J	4	ISM38 ISM39 ISM68 ISM69	AAV1.CAG.Flex.eGFP.WPRE.bGH (AV-1-ALL854)	2×4μA/3min 2×4μA 10–12min 5–6μA 10min	34–55	Anterograde: GAD65	PHOX2b ISM 38&39 EGFP ISM 68&69
GAD65-cre (hom) GAD65-cre (het)	As above As above	1 1	SL15–71 ISM51	AAV1.CBA.Flex.ChR2(H134R)-mCherry.WPRES.SV40 (AV-1-18916P) AAV1.CBA.Flex.ChR2 (H134R)-mCherry.WPRES.SV40 AV-1-18916P)	10μA/ 12min 4μA/10min	32 31	Anterograde: GAD65 Anterograde: GAD65	mCherry mCherry PHOX2b
DBH-cre (het)	B6.FVB(Cg)-TG(Dbh-cre) KH212Gsat/Mmucd (RRID MMRRC_03677 8-UCD) × C57BL6/J	2	ISM59 ISM72[†]	AAV1.CAG.Flex.eGFP.WPRE.bGH AV-1-ALL854)	4μA×10–15min	19–26	Anterograde: DBH	EGFP/TH double EGFP DAB
DBH-cre (het)	As above	1	ISM90	AAV1.CBA.Flex.ChR2 (H134R)-mCherry.WPRES.SV40 AV-1-18916P)	Pressure: ~80nl	67	Anterograde: DBH	mCherry DAB

[†]Denotes cases illustrated in figures

[‡]All 19 mice were adults. Ages at perfusion ranged from 68–245 days, for the 13/19 mice where this information was available

[§]Mice of both genders were used. For the 17 cases where gender was noted, 8 mice were females and 9 males

¶All heterozygous crosses were made with C57BL/6

TABLE 2

RETROGRADE TRACER INJECTIONS[†,‡]

Strain[§]	Mouse ID	Tracer	Injection	Survival (d)	Immunohistochemistry
GAD67-EGFP+	ISM3	FG	~1uA/15 min	7	FG
GAD67-EGFP+	ISM4[†]	FG	2–8Ua/15 min	9	FG/PHOX2b FG/TH
GAD67-EGFP+	ISM5	FG	1–8uA/15min	10	FG/TH
GAD67-EGFP+	ISM8	FG	1–8uA/15min	13	FG/TH
GAD67-EGFP−	ISM10	FG	5uA/15 min	8	FG/TH FG/PHOX2b
GAD67-EGFP−	ISM13	FG	Not noted4	10	FG/TH FG/PHOX2b
GAD67-EGFP+	ISM17	FG	5 min[4]	8	FG/TH FG/PHOX2b
GAD67-EGFP+	ISM18	FG	3–5uA/2 min	6	FG(r)/TH
GAD67-EGFP+	ISM19	FG	2.5 min[4]	5	FG/TH

[†]denotes case used in Figure 9

[‡]All 9 mice were adults. Weights ranged from 27–47 gr. In the 8 cases where gender was noted, 7 mice were males and 1 was a female. In a few instances, injection parameters were not noted but were within the range reported for the other cases

[§]All mice were heterozygous offspring of C57BL6/J and GAD67-GFP knockin mice (RRID:IMSR_RBRC03674) (Tamamaki et al., 2003)

[¶]Abbreviations: FG- Fluorogold, TH- tyrosine hydroxylase

TABLE 3

PRIMARY ANTIBODIES

Antibody/clonality	Immunogen	Manufacturer/catalog # Lot	RRID	Working dilution
Rabbit anti-fluorogold polyclonal	KLH-conjugated Fluorescent Gold	Millipore 153 Lot: LV1644476	RRID: AB_90738	1:10,000
Guinea pig anti-fluorogold polyclonal	Glutaraldehyde-conjugated fluorogold	Protos Biotech/NM-101 Flu Ggp No lot number	RRID: AB_2314409	1:1000
Rabbit Anti-tyrosine hydroxylase polyclonal	Denatured tyrosine hydroxylase from rat pheochromocytoma (denatured by sodium dodecyl sulfate).	Millipore AB152 Lot: 1861503	RRID: AB_390204	1:1000
Sheep Anti-tyrosine hydroxylase polyclonal	Native tyrosine hydroxylase from rat pheochromocytoma (J. Biol. Chem., 1982, 257:9416–9423).	Millipore AB1542 Lot: 1994656	RRID:AB_90755	1:1000
Anti-EGFP polyclonal	GFP isolated directly from the jellyfish Aequorea victoria.	Invitrogen/ Life technologies /Molecular Probes A11122	RRID: AB_221569 Lot: 1356608	1:50,000 (DAB) 1:15,000 fluorescence
Rabbit Anti-PHOX2b polyclonal	C terminal; 14 AA with added tyrosine; YFHRKPGPALKTNLF; (Pattyn et al., 1997)	Gift: Jean-Francois Brunet	RRID: AB_2315161 or RRID: AB_2315160	1:1000
Rabbit Anti-P2×2 polyclonal	Peptide (C)SQQDSTSTDPKGLAQL, corresponding to amino acid residues 457–472 of rat P2×2 Receptor (Accession P49653). Intracellular, C-terminus.	Alomone APR-003 Lot: AN09	RRID: AB_2040054	1:10000
Rabbit m-Cherry (called DSRed by clontech) polyclonal	DsRed-Express, a variant of Discosoma sp. red fluorescent protein	Clontech/632496 Lot: 1306037	RRID: AB_10013483	1:5000